THE PRACTICAL CALCULATION OF THE AERODYNAMIC
CHARACTERISTICS OF SLENDER FINNED VEHICLES

by

James. S. Barrowman

A Dissertation Submitted to the Faculty of the School of Engineering and Architecture of The Catholic University of America in Partial Fulfillment of the Requirements for the Degree of Master of Science in Aerospace Engineering.

March 1967

Washington, D. C.

This dissertation was approved by _____
$\hspace{6cm}$ Dr. Shu J. Ying

Assistant Professor of Space Science and Applied Physics

as Director and by _____
$\hspace{5cm}$ Dr. Hsing-Ping Pao

as Reader.

ACKNOWLEDGMENTS

TABLE OF CONTENTS

LIST OF FIGURES

LIST OF SYMBOLS

Symbol	Description
A	Area
A_B	Base Area
A_{B_f}	Base Area of One Fin
A_{B_N}	Nose Base Area
A_{B_S}	Conical Shoulder or Boattail Base Area
A_r	Reference Area
A_T	Planform Area of One Exposed Fin Panel
A_{W_B}	Total Body Wetted Area
$A_{W_{BA}}$	Wetted Area of Booster Nose Afterbody
A_{W_N}	Nose Wetted Area
$A_{W_{NA}}$	Wetted Area of Sustainer Nose and the Cylindrical Afterbody Between the Nose and the Shoulder. If there is no Shoulder, the Afterbody is Taken as the Remainder of the Sustainer.
A_{W_S}	Conical Shoulder or Boattail Wetted Area
$A_{W_{SA}}$	Wetted Area of the Shoulder or Bottail and the Portion of the Sustainer Aft of the Shoulder or Boattail
$\mathbb{R}$	Aspect Ratio of Exposed Fin
a	Ambient Speed of Sound
B_3	Third Order Busseman Irreversibility Coefficient
C_D	Drag Coefficient, $\dfrac{D}{\bar{q}\,A_r}$
C_{D_B}	Base Drag Coefficient
$C_{D_{BT}}$	Tail Trailing Edge Drag Coefficient
C_{D_f}	Skin Friction Drag Coefficient
$C_{D_{LT}}$	Tail Leading Edge Drag Coefficient
C_{D_P}	Pressure Drag Coefficient
C_{D_T}	Total Drag Coefficient
$C_{D_{TT}}$	Tail Thickness Drag Coefficient
C_{D_W}	Wave Drag Coefficient

Symbol	Description
C_f	Incompressible Skin Friction Coefficient
C_{f_c}	Compressible Skin Friction Coefficient
C_1	Rolling Moment Coefficient, $\bar{\ell}/\bar{q} A_r L_r$
C_{1_p}	Roll Damping Moment Coefficient Derivative, $\partial C_\ell/\partial \left(\dfrac{PL_r}{2V}\right)$ @ $\dfrac{PL_r}{2V} = 0$
C_{1_δ}	Roll Forcing Moment Coefficient Derivative, $\partial C_\ell/\partial \delta$ @ $\delta = 0$
C_m	Pitch Moment Coefficient, $\bar{m}/\bar{q} A_r L_r$
C_{m_q}	Pitch Damping Moment Coefficient Derivative, $\partial C_m/\partial \left(\dfrac{qL_r}{2V}\right)$ @ $\dfrac{qL_r}{2V} = 0$
C_N	Normal Force Coefficient, $n/\bar{q} A_r$
C_{N_α}	Normal Force Coefficient Derivative, $\partial C_N/\partial \alpha$ @ $\alpha = 0$
C_P	Pressure Coefficient, $\Delta P/\bar{q}$
c	Cord Length
c_{MA}	Mean Aerodynamic Chord
c_r	Fin Root Chord
c_t	Fin Tip Chord
D	Aerodynamic Drag Force
d	Diameter
d_N	Diameter of Nose Base
d_S	Diameter of Shoulder or Boattail Base
F	Force
f_B	Total Body Fineness Ratio
F_D	Diederich's Planform Correlation Parameter for Fins
f_e	Equivalent Fineness Ratio of a Truncated Cone
f_N	Nose Fineness Ratio
f_{N_A}	Fineness Ratio of the Nose and Nose Afterbody
f_{S_A}	Fineness Ratio of the Shoulder or Boattail and Shoulder Afterbody
h	Fin Trailing Edge Thickness
K, k	Interference Factors and General Constants
K_1	First Order Busseman Coefficient
K_2	Second Order Busseman Coefficient

Symbol	Description
K_3	Third Order Busseman Coefficient
L	Length
L_r	Reference Length
1_{A_F}	Location of Shoulder or Bottail Measured from the Nose Tip
1_{L_R}	Fin Root Leading Edge Wedge Length
1_N	Nose Length
1_0	Total Body Length
1_s	Shoulder or Bottail Length
1_T	Location of Fin Leading Edge Intersection with Body, Measured from Nose Tip
1_{T_R}	Fin Root Trailing Edge Wedge Length
$\bar{l}$	Roll Moment About Longitudinal Axis
M	Mach Number
m	Cotangent Γ_L
$\bar{m}$	Pitch Moment About Center of Gravity
N	Number of Fins (3 or 4)
n	Normal Aerodynamic Force
P_r	Prandtle Factor, $1/\sqrt{1 - M^2}$
P_f	Prandtle Factor for Swept Fins, $1/\sqrt{1 - M^2 \cos^2 \Gamma_c}$
p	Roll Rate
q	Pitch Rate
$\bar{q}$	Dynamic Pressure
R_e	Reynolds Number
R_s	Surface Roughness Height
r_L	Fin Leading Edge Radius
r_t	Body Radius at Tail
S	Exposed Fin Semispan Measured from Root Chord
t	Maximum Fin Thickness
V	Velocity
V_B	Body Volume
w	Downwash Velocity

Symbol	Description
X_{CG}	Center of Gravity Location Measured from Nose Tip
X_{L_T}	Distance Between Fin Root Leading Edge and the Fin Tip Leading Edge Measured Parallel to the Root
$\bar{X}$	Longitudinal Center of Pressure Location Measured from Nose Tip
$\bar{Y}$	Spanwise Center of Pressure Location Measured from the Longitudinal Axis
Y_{MA}	Spanwise Location of C_{MA} Measured from the Root Chord
α	Angle of Attack
β	Supersonic, $\sqrt{M^2 - 1}$; Subsonic, $\sqrt{1 - M_2}$
Γ_c	Midchord Line Sweep Angle
$\Gamma_{1/4}$	Quarter Chord Sweep Angle
Γ_L	Leading Edge Sweep Angle
Γ_T	Trailing Edge Sweep Angle
Γ_1	First Region Boundary Sweep Angle
Γ_2	Second Region Boundary Sweep Angle
γ	Ratio of Specific Heats
ζ_L	Fin Leading Edge Wedge Half Angle in a Plane Parallel to the Flow
ζ_T	Fin Trailing Edge Wedge Half Angle in a Plane Parallel to the Flow
η	Incidence of Surface to Flow in a Plane Parallel to the Flow
Λ	Fin Dihedral Angle
λ	Fin Taper Ratio, c_t / c_r
μ	Mach Angle
ν	Ambient Kinematic Viscosity
ρ	Ambient Density
σ	Nose Tip Half Angle
τ	$\dfrac{s + r_t}{r_t}$ Ratio

Subscripts

B	Body
B(T)	Body in the Presence of the Tail
cr	Critical Value
N	Nose
r	Root
S	Conical Shoulder or Boattail
T	Tail
T(B)	Tail in the Presence of the Body
t	Tip
W	Wetted
1	Value for one fin

1.00 SYNPOSIS

The basic objective of this thesis is to provide a practical method of computing the aerodynamic characteristics of slender finned vehicles such as sounding rockets, high speed bombs, and guided missiles. The aerodynamic characteristics considered are the normal force coefficient derivative, C_{N_α}; center of pressure, $\bar{X}$; roll forcing moment coefficient derivative, C_{ℓ_δ}; roll damping moment coefficient derivative, C_{ℓ_p}; pitch damping moment coefficient derivative, C_{m_q}; and the drag coefficient, C_D. Equations are determined for both subsonic and supersonic flow. No attempt is made to analyze the transonic region. The general configuration to which the relations are applicable is a slender axisymmetric body having three or four fins.

The fins and body are analyzed separately; and the interference between them is accounted for when they are combined to form the total vehicle. When necessary, both the fins and the body are subdivided. Both purely theoretical and semi-empirical methods are used in deriving the equations. Use is made of established methods when they are applicable.

Since the high speed digital computer is a tool readily available to the contempory engineer, no effort has been made to linearize higher order theories or simplify complex relations. In many cases, the equations are derived with the computer in mind.

The method is applied to sounding rocket vehicles and the results are compared to respective windtunnel and flight data. The comparison indicates that the theory predicts aerodynamic characteristics within ten percent of the experimental data.

2.00 INTRODUCTION

2.10 BACKGROUND

In order to study the performance of a new or existing flight vehicle the engineer must have the vehicles aerodynamic characteristics. Windtunnel or flight tests can provide the needed information; but they are both expensive and time consuming. Lacking either time or money the engineer turns to theoretical predictions.

In this day of rockets and high speed armaments, slender finned vehicles are of considerable interest. A great deal of work has been done on the aerodynamics of such configurations. The list of contributors is exhaustive. However, a number of works stand out and are of particular interest. Munk, reference 20, developed the technique of slender body theory and applied it to low speed airships. Tsien, reference 29, later modified Munks technique to apply it to pointed projectiles in supersonic flow. Jones, references 7, 8, 9, extended Munk's work to finite wings and also provided excellent application of conical flow theory to wing lift and drag estimation. Nielsen, Pitts, Ferrari, and Morikawa, references 22, 3, 18 and 17, have thoroughly analyzed wing-body interference effects.

Even though they provide valuable understanding, many of the contributions have limited applicability to practical calculations. Their inherent assumptions and approximations reduce the accuracy and reliability of their results. Those that provide accuracy are usually so complex or

1

abstract they cannot directly provide the desired aerodynamic characteristics. This thesis is an attempt to form concrete, useful expressions by applying the best abstract theoretical treatments as well as reliable empirical data.

2.20 STATEMENT OF PROBLEM

Determine a set of expressions for the practical calculation of the aerodynamic characteristics of slender, axisymmetric finned vehicles at both subsonic and supersonic speeds. The characteristics of interest are the normal force coefficient derivative, C_{N_α}; center of pressure, $\bar{X}$; roll forcing moment coefficient derivative, C_{ℓ_δ}; roll damping moment coefficient derivative, C_{ℓ_p}; pitch damping moment coefficient derivative, C_{m_q}; and drag coefficient, C_D.

2.30 GENERAL METHOD OF SOLUTION

1. Divide vehicle into body and tail.
2. Analyze the body and tail separately. Subdivide either when necessary.
3. Analyze wing-body interference.
4. Recombine to form total vehicle solution.

2.40 GENERAL ASSUMPTIONS

1. The angle-of-attack is very near zero.
2. The flow is steady and irrotational.
3. The vehicle is a rigid body.
4. The nose tip is a sharp point.

3.0 NORMAL FORCE AERODYNAMICS

There are a number of aerodynamic coefficient derivatives that are directly dependent on the aerodynamic forces acting normal to the longitudinal axis of the vehicle. The normal forces acting on the fins are generated by four main sources; angle-of-attack; fin cant angle, roll rate, and pitch rate. These excitations produce the normal force coefficient derivative, C_{N_α}, at a center of pressure, $\bar{X}$ & $\bar{Y}$; a roll forcing moment coefficient derivative, C_{ℓ_δ}; a roll damping moment coefficient derivative, C_{ℓ_p}; and a pitch damping moment coefficient derivative, C_{m_q} respectively. The only normal force acting on the body is due to the angle of attack. This is the normal force at a center of pressure.

3.10 TAIL NORMAL FORCE AERODYNAMICS

3.11 TAIL NORMAL FORCE COEFFICIENT DERIVATIVE

In subsonic flow, the semi-empirical method of Diederich from reference 2 gives the normal force coefficient derivative of a finite thin plate as;

$$\left(C_{N_\alpha}\right)_1 = \frac{C_{N_{\alpha 0}} \, F_D \left(\dfrac{A_f}{A_r}\right) \cos \Gamma_c}{2 + F_D \sqrt{1 + \dfrac{4}{F_D^2}}} \tag{3-1}$$

where;

$C_{N_{\alpha 0}}$ = Normal Force Coefficient Derivative of a two dimensional airfoil.

F_D = Diederich's Planform Correlation Parameter.

According to Diederich;

$$F_D = \frac{\text{\AE}}{\dfrac{1}{2\pi} C_{N_{\alpha 0}} \cos \Gamma_c} \tag{3-2}$$

By the thin airfoil theory of potential flow (reference 26),

$$C_{N_{\alpha 0}} = 2\pi \tag{3-3}$$

Correcting this for compressible flow according to Gothert's rule (reference 26)

$$C_{N_{\alpha 0}} = \frac{2\pi}{\beta} \tag{3-4}$$

Thus;

$$F_D = \frac{\beta \, \text{\AE}}{\cos \Gamma_c} \tag{3-5}$$

Substituting equations (3-4) and (3-5) into (3-1) and simplifying,

$$\left(C_{N_\alpha}\right)_1 = \frac{2\pi \, \text{\AE} \, (A_f / A_r)}{2 + \sqrt{4 + \left(\dfrac{\beta \, \text{\AE}}{\cos \Gamma_c}\right)^2}} \tag{3-6}$$

This is the value for one fin.

The value of $\left(C_{N_\alpha}\right)_T$ for one fin in supersonic flow is computed using the method of reference 1, as given in Appendix A. It is essentially a strip theory which analyses two dimensional strips using Busemann's Third order expansion of the compressible flow equations.

$$C_{P_i} = K_1 \, \eta_i + K_2 \, \eta_i^2 + K_3 \, \eta_i^3 + B_3 \, \eta_L^3 \tag{3-7}$$

where;

$$K_1 = 2/\beta$$

$$K_2 = \frac{(\gamma + 1) \, M^4 - 4\beta^2}{4\beta^4}$$

3

$$K_3 = \frac{(\gamma + 1) M^8 + (2\gamma^2 - 7\gamma - 5) M^6 + 10(\gamma + 1) M^4 - 12 M^2 + 8}{6 \beta^7}$$

$$B_3 = (\gamma + 1) M^4 [(5 - 3\gamma) M^4 + 4(\gamma - 3) M^2 + 8] \frac{1}{48}$$

The strip values are then summed in a spanwise direction with a correction applied to those strips that are intersected by the fin tip mach cone. The most distinct advantage of the method in reference 1 is that it includes a thickness distribution in the analysis.

To apply the C_{N_α} of one fin to a multi-finned vehicle the effect of fin dihedral must be considered. Only three and four finned vehicles are analyzed, since these are the most commonly used. Both are analysed assuming that one fin is in a plane parallel to the flow. Reference 13 derives the effect of dihedral on the C_{N_α} of two fin panels at very small angles of attack.

$$\left(C_{N_\alpha}\right)_t = 2 \left(C_{N_\alpha}\right)_1 \cos^2 \Lambda \qquad (3-8)$$

Figure 3-1 defines the dihedral angle, Λ.

A three (3) fin configuration has two effective panels at a 30° dihedral angle. Thus the tail normal force derivative is,

$$\left(C_{N_\alpha}\right)_T = 2 \left(C_{N_\alpha}\right)_1 \cos^2 30°$$

$$= 2 \left(C_{N_\alpha}\right)_1 \left(\frac{\sqrt{3}}{2}\right)^2$$

$$\left(C_{N_\alpha}\right)_T = \frac{3}{2} \left(C_{N_\alpha}\right)_1 \qquad \text{(3 fins)} \qquad (3-9)$$

Since the dihedral angle of the two effective panels of a four (4) fin configuration is zero, the tail normal force derivative is;

$$\left(C_{N_\alpha}\right)_T = 2 \left(C_{N_\alpha}\right)_1$$

$$\left(C_{N_\alpha}\right)_T = \frac{4}{2} \left(C_{N_\alpha}\right)_1 \qquad \text{(4 fins)} \qquad (3-10)$$

From equations 3-9 and 3-10 we can generalize for three and four fin vehicles.

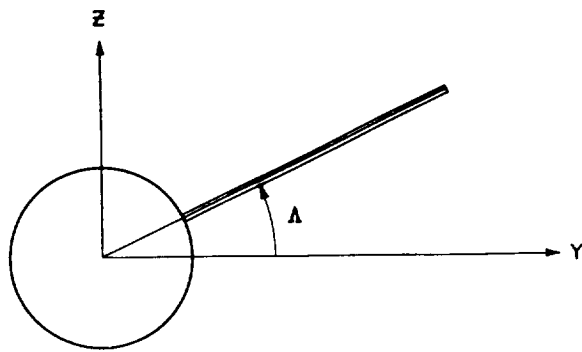$$\left(C_{N_\alpha}\right)_T = \frac{N}{2} \left(C_{N_\alpha}\right)_1 \qquad (3-11)$$

4

Figure 3-1—Fin Dihedral Angle (As Viewed From Rear)

Substituting 3-6 into 3-11, for subsonic flow;

$$\left(C_{N_\alpha}\right)_T = \frac{N \pi R \left(A_f/A_r\right)}{2 + \sqrt{4 + \left(\dfrac{\beta R}{\cos \Gamma_c}\right)^2}}$$

(3-12)

3.12 TAIL CENTER OF PRESSURE LOCATION

From the thin airfoil theory of subsonic potential flow, reference 26, the center of pressure of a two dimensional airfoil is located at 1/4 the length of its chord from its leading edge. Thus, on a three dimensional fin, the center of pressure is located along the quarter chord line. By definition, the center of pressure is also located along the mean aerodynamic chord of the fin. Therefore, by the above argument, the subsonic fin center of pressure is located at the intersection of the quarter chord line and the mean aerodynamic chord. In this treatment, the subsonic center of pressure is considered to remain constant with mach number. It remains to determine the length and position of the mean aerodynamic chord.

The mean aerodynamic chord is defined as;

$$c_{MA} = \frac{1}{A_f} \int_0^s c^2 \, dy$$

(3-13)

Figure 3-2 shows the fin coordinate system. The generalized chord is a function of the spanwise coordinate. To find this function, a proportionality relation is set up. See figure 3-3.

$$\frac{c_r}{L^*} = \frac{c}{L - y} = \frac{c_t}{L^* - s}$$

(3-14)

It is assumed that the fin edges are all straight and form a trapizoid. From the first two terms of equation 3-14;

$$c = c_r - \frac{y}{L^*} c_r$$

(3-15)

From the first and last terms of equation 3-14;

$$C_t L^* = c_r L^* - c_r S$$

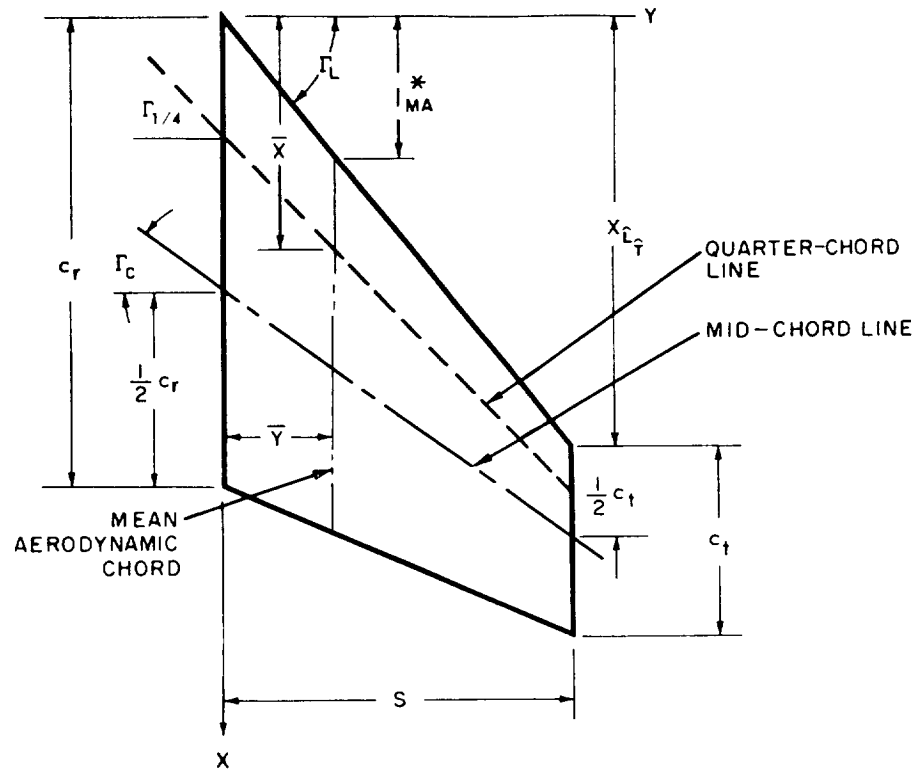Simplifying, and defining;

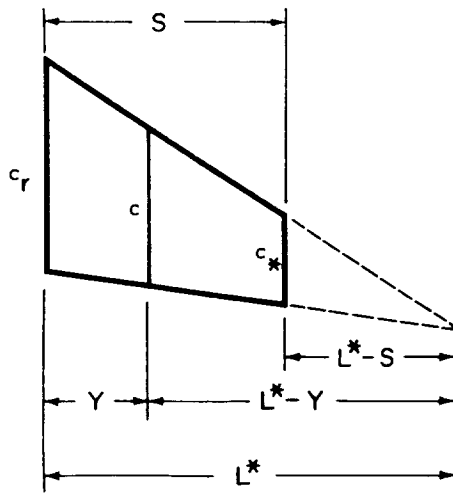$$\lambda = \frac{c_t}{c_r}$$

(3-16)

6

Figure 3-2—Fin Geometry

Figure 3-3—Proportionality Triangle for Chord

we find;

$$L^* = \frac{s}{1 - \lambda} \qquad (3\text{-}17)$$

Substituting 3-17 into 3-15,

$$c = c_r (1 + ky) \qquad (3\text{-}18)$$

where,

$$k = \frac{1}{L^*} = \frac{\lambda - 1}{s} \qquad (3\text{-}19)$$

Using 3-18 in 3-13;

$$c_{MA} = \frac{c_r^2}{A_f} \int_0^s (1 + ky)^2 \, dy \qquad (3\text{-}20)$$

Integrating

$$c_{MA} = \frac{c_r^2}{A_f \, 3k} \left[(1 + ks)^3 - 1 \right]$$

$$c_{MA} = \frac{c_r^2 \, s}{A_f} \left[1 + ks + \frac{1}{3} k^2 s^2 \right] \qquad (3\text{-}21)$$

Substituting 3-19 into 3-21 and simplifying;

$$c_{MA} = \frac{1}{3} \frac{c_r^2 \, s}{A_f} \left[\lambda^2 + \lambda + 1 \right] \qquad (3\text{-}22)$$

But;

$$A_f = \frac{1}{2} (c_r + c_t) \, s \qquad (3\text{-}23)$$

thus;

$$c_{MA} = \frac{2}{3} \frac{c_r^2}{c_r + c_t} \left[\lambda^2 + \lambda + 1 \right]$$

9

or,

$$c_{MA} = \frac{2}{3} \left[c_r + c_t - \frac{c_r c_t}{c_r + c_t} \right]$$ (3-24)

To find the spanwise location of c_{MA}, equate 3-24 and 3-18 and solve for y.

$$\frac{2}{3} \left[c_r + c_t - \frac{c_r c_t}{c_r + c_t} \right] = c_r \left[1 + \frac{\lambda - 1}{s} y \right]$$

or

$$Y_{MA} = \left[\frac{2}{3} (c_r + c_t) - \frac{2 c_r c_t}{3(c_r + c_t)} - c_r \right] \frac{s}{c_r - c_t}$$ (3-25)

After much algebra;

$$Y_{MA} = \frac{s}{3} \left[\frac{c_r + 2 c_t}{c_r + c_t} \right]$$ (3-26)

The spanwise subsonic center of pressure coordinate is then;

$$\overline{Y}_T = r_t + \frac{s}{3} \left[\frac{c_r + 2 c_t}{c_r + c_t} \right]$$ (3-27)

As can be seen from figure 3-1, the longitudinal coordinate is;

$$\overline{X}_T = 1_T + 1_{MA} + \frac{1}{4} c_{MA}$$ (3-28)

But;

$$1_{MA} = y_{MA} \tan \Gamma_L = \frac{y_{MA}}{s} x_t$$ (3-29)

Combining equations 3-24, 3-26, 3-28, and 3-29;

$$\overline{X}_T = 1_T + \frac{x_t}{3} \left[\frac{c_r + 2 c_t}{c_r + c_t} \right] + \frac{1}{6} \left[c_r + c_t - \frac{c_r c_t}{c_r + c_t} \right]$$ (3-30)

The fin center of pressure in supersonic flow is found by the method of reference 1 in appendix A.

10

3.13 TAIL ROLL FORCING MOMENT COEFFICIENT DERIVATIVE

A force arises on a fin at zero angle of attack if the fin is canted at an angle with the longitudinal axis. See figure 3-4. The cant angle is an effective angle-of-attack. As can be seen in figure 3-5, the total force resulting from canting all the fins at the same angle is zero on three and four fin configurations. However, a roll forcing moment about the longitudinal axis is produced. Since the cant angle acts as an effective angle of attack the roll forcing moment is subsonic flow may be written in terms of $\left(C_{N_\alpha}\right)_1$;

$$\bar{1} = N \, \bar{Y}_T \, \left(C_{N_\alpha}\right)_1 \delta \, \bar{q} \, A_r \tag{3-31}$$

The values of $\left(C_{N_\alpha}\right)_1$ and $\bar{Y}_T$ are found using equations 3-6 and 3-27 respectively. The rolling moment coefficient is defined as,

$$C_\ell = \frac{\bar{1}}{\bar{q} \, A_r \, L_r} \tag{3-32}$$

thus; using equation 3-26;

$$C_\ell = \frac{N \, \bar{Y}_T \, C_{N_\alpha 1} \, \delta}{L_r} \tag{3-33}$$

The roll forcing moment coefficient derivative is defined as;

$$C_{\ell_\delta} = \left. \frac{\partial C_\ell}{\partial \delta} \right|_{\delta = 0} \tag{3-34}$$

thus; the subsonic roll forcing coefficient derivative is,

$$C_{\ell_\delta} = N \, \left(C_{N_\alpha}\right)_1 \frac{\bar{Y}_T}{L_r} \tag{3-35}$$

In supersonic flow, C_{ℓ_δ} is computed using the method of reference 1 as given in appendix A. This method determines the roll forcing moment of each strip and sums them in a spanwise direction.

3.14 TAIL ROLL DAMPING MOMENT COEFFICIENT DERIVATIVE

When the vehicle has a roll velocity, the superposition of the local tangential velocity of the fin panel on the free stream velocity produces a local angle-of-attack which is a function of spanwise position. The local angle-of-attack produces a local force distribution along the fin. For three and four fin configurations the total resulting force is zero, as shown previously. The moment produced about the longitudinal axis opposes the roll rate (see figure 3-6) and is a roll damping moment. The local rolling moment at $\bar{s}$ is,
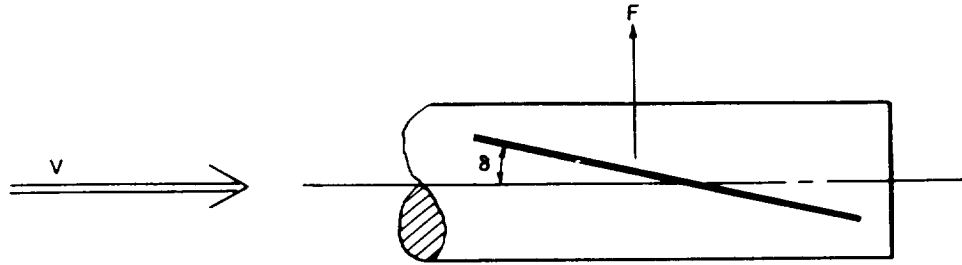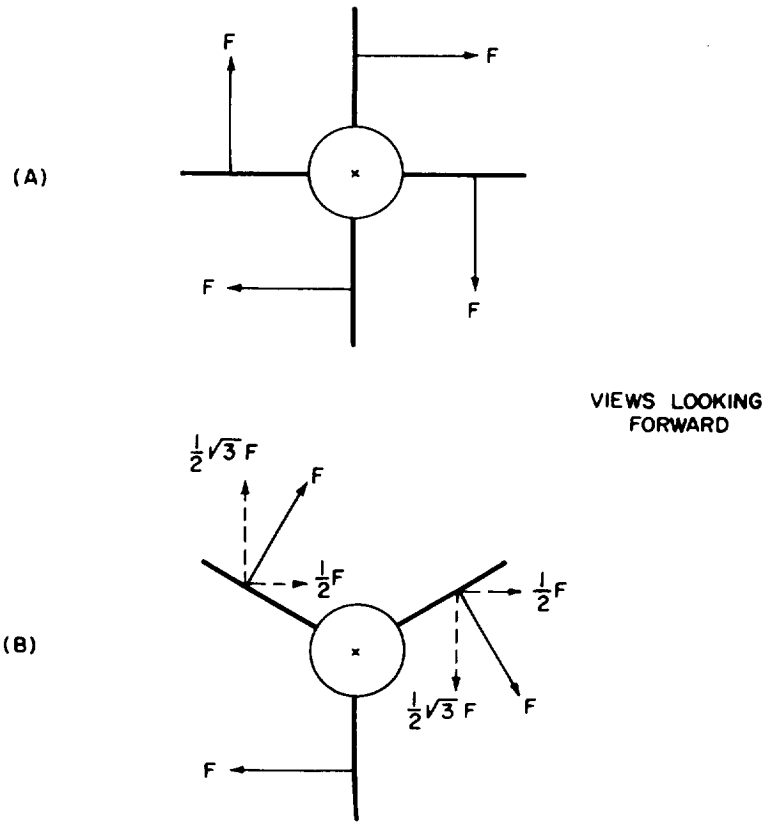
Figure 3-4—Fin Cant Angle

(A)

(B)

Figure 3-5—Forces Due to Fin Cant
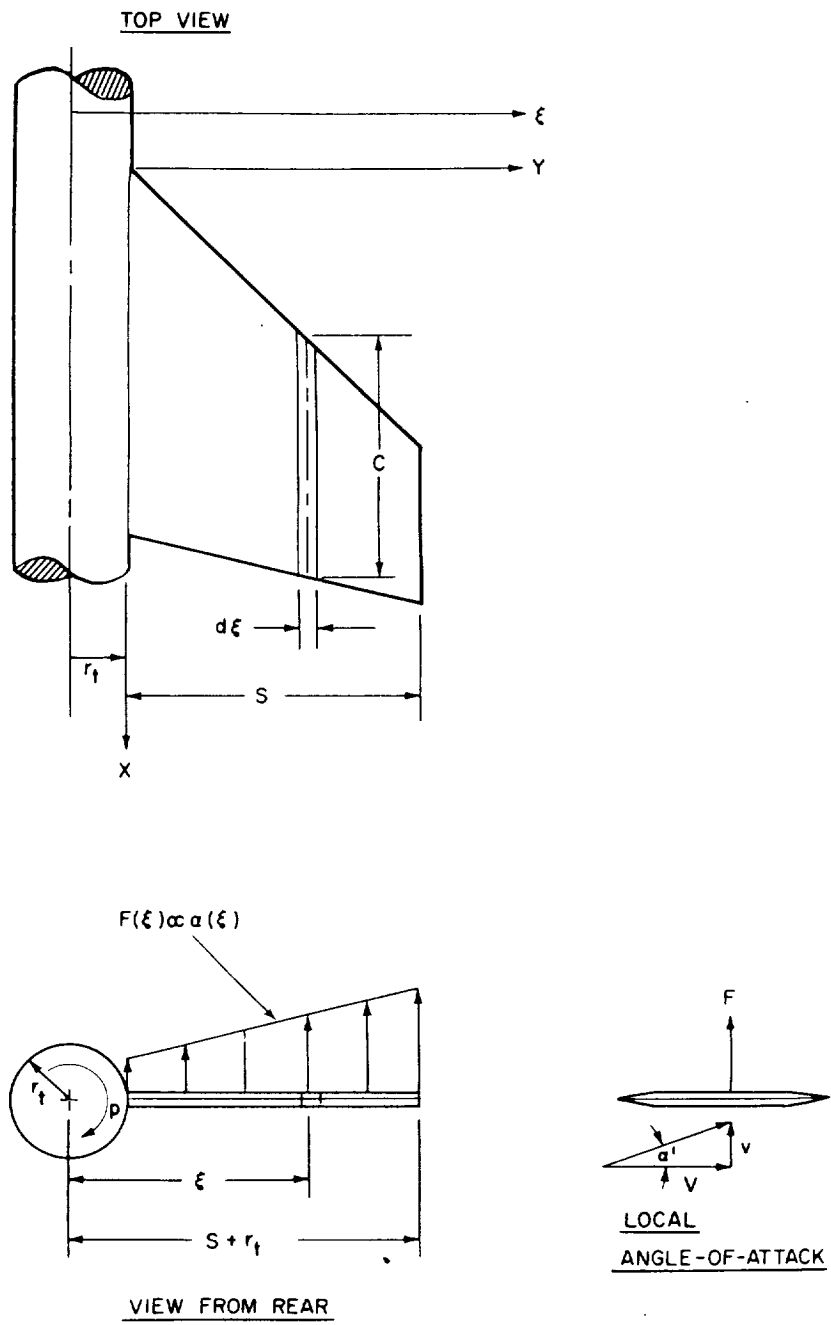
13

TOP VIEW

Figure 3-6—Roll Damping Parameters

14

$$d\bar{l} = \xi F(\xi) \tag{3-36}$$

The local angle of attack at ξ is,

$$\alpha(\xi) = \tan^{-1}\left(\frac{v(\xi)}{V}\right) \tag{3-37}$$

But;

$$v(\xi) = -P\xi$$

Thus;

$$\alpha(\xi) = \tan^{-1}\left(-\frac{P\xi}{V}\right) \tag{3-38}$$

For $V \gg P\xi$ the local angle-of-attack is near zero, thus;

$$\alpha(\xi) = -\frac{P\xi}{V} \tag{3-39}$$

In subsonic compressible flow the local normal force on an airfoil strip is found using equation 3-4.

$$F(\xi) = C_{N_{\alpha 0}} \bar{q} \alpha(\xi) c(\xi) d\xi \tag{3-40}$$

Where $C_{N_{\alpha 0}}$ is defined in equation 3-4. Knowing that,

$$y = \xi - r_t \tag{3-41}$$

equation 3-18 gives

$$c(\xi) = c_r\left[1 - \frac{1-\lambda}{s}(\xi - r_t)\right]$$

or

$$c(\xi) = \frac{c_r(1-\lambda)}{s}\left(\frac{s}{1-\lambda} - \xi + r_t\right) \tag{3-42}$$

15

Combining equations 3-36, 3-39, 3-40, and 3-42;

$$d\bar{l} = \xi \, C_{N_{\alpha 0}} \, \bar{q} \, \left(-\frac{P\xi}{V}\right) \left[\frac{c_r (1-\lambda)}{s} \left(\frac{s}{1-\lambda} - \xi + r_t\right)\right] d\xi$$

Simplifying;

$$d\bar{l} = -\frac{C_{N_{\alpha 0}} \, \bar{q} \, p c_r \, (1-\lambda)}{VS} \, (L^* + r_t - \xi) \, \xi^2 \, d\xi \tag{3-43}$$

where L^* is defined by equation 3-17. Applying equation 3-32 provides the local roll moment coefficient.

$$dC_\ell = -\frac{C_{N_{\alpha 0}} \, P c_r \, (1-\lambda)}{A_r \, L_r \, VS} \, (L^* + r_t - \xi) \, \xi^2 \, d\xi \tag{3-44}$$

Integrating over the exposed fin,

$$C_\ell = k \int_{r_t}^{s+r_t} [(L^* + r_t) - \xi] \, \xi^2 \, d\xi \tag{3-45}$$

where;

$$k = -\frac{p c_r \, (1-\lambda) \, C_{N_{\alpha 0}}}{A_r \, L_r \, VS} \tag{3-46}$$

Performing the integration;

$$C_\ell = \frac{k \, s^2}{12(1-\lambda)} \, [(1+3\lambda) \, s^2 + 4(1+2\lambda) \, s r_t + 6(1+\lambda) \, r_t^2] \tag{3-47}$$

Reintroducing k and simplifying;

$$C_\ell = -\frac{p c_r \, s \, C_{N_{\alpha 0}}}{12 \, \beta \, A_r \, L_r \, V} \, [(1+3\lambda) \, s^2 + 4(1+2\lambda) \, s r_t + 6(1+\lambda) \, r_t^2] \tag{3-48}$$

The roll damping moment coefficient derivative is defined as;

$$C_{\ell_p} = \frac{\partial C_\ell}{\partial \left(\frac{PL_r}{2V}\right)}\Bigg|_{\frac{PL_r}{2V}=0} \tag{3-49}$$

16

Then, from 3-48,

$$C_{\ell_p} = - \frac{c_r S C_{N_{\alpha 0}}}{6 L_r^2 A_r} [(1 + 3\lambda) s^2 + 4(1 + 2\lambda) s r_t + 6(1 + \lambda) r_t^2] \tag{3-50}$$

However, $C_{N_{\alpha 0}}$ must be corrected for three dimensional effects using the Diederich correlation parameter. From the results of section 3.11, equations 3-1, 3-5, and 3-6, the subsonic roll damping moment coefficient derivative for N fins is,

$$C_{\ell_p} = - \frac{N c_r S}{6 L_r^2} [(1 + 3\lambda) s^2 + 4(1 + 2\lambda) s r_t + 6(1 + \lambda) r_t^2] \left(C_N \right)_1 \tag{3-51}$$

In order to determine the roll damping moment coefficient derivative in supersonic flow, the angle-of-attack distribution of equation 3-37 is introduced into the equations of reference 1 in appendix A. The resulting rolling moment is divided by $PL_r / 2V$ to form the roll damping derivative. To insure that C_{ℓ_p} is truely a linear derivative, the value of α_{max} must be near zero. To provide this condition we assume

$$\frac{PL_r}{2V} = k \tag{3-52}$$

where k is any defined constant; and,

$$k << 1$$

From equations 3-37 and 3-41:

$$\alpha_{max} = \tan^{-1} \left[- \frac{p(s + r_t)}{V} \right]$$

Using equation 3-52,

$$\alpha_{max} = \tan^{-1} \left[- \frac{2k(s + r_t)}{L_r} \right] \tag{3-53}$$

For the slender, finned vehicles under consideration:

$$\frac{2(s + r_t)}{L_r} \approx 4$$

Thus

$$\alpha_{max} = \tan^{-1} (4k) \tag{3-54}$$

17

To satisfy the criterion,

$$\alpha \approx \tan \alpha$$

equation 3-54 dictates that,

$$k \leq 10^{-3}$$

Using the equality, the angle-of-attack variation becomes;

$$\alpha(y) = -\frac{.002 (y \cdot r_t)}{L_r} \tag{3-55}$$

This variation is introduced into the equations of reference 1 and a value of the damping C is determined. The corresponding C_{ℓ_δ} is found by,

$$C_{\ell_p} = \frac{C_{\ell_\delta}}{\left(\dfrac{PL_r}{2V}\right)} = \frac{C_{\ell_\delta}}{k} = 1000 \, C_{\ell_\delta}$$

For N fins;

$$C_{\ell_p} = 1000 \, N \, C_{\ell_\delta} \tag{3-56}$$

3.20 BODY NORMAL FORCE COEFFICIENT DERIVATIVE

3.21 BODY NORMAL FORCE DERIVATIVE

The axisymmetric body of a slender vehicle is generally a combination of a nose shape, circular cylinders and conical frustrums. The nose shape is usually conical or tangent ogival. See figure 3-7. It is required that there be no discontinuities at the interfaces of these components. This allows integration over the entire length of the body. The effect of compressibility in subsonic flow will not be considered in this analysis. From a static stability point of view, this is a conservative assumption since the normal force coefficient derivative increases near mach one.
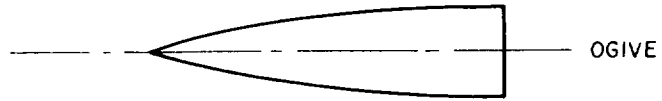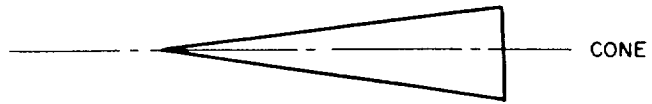
For a slender axially symmetric body in subsonic flow, references 15 and 4 derive the steady state running normal load as,

$$n(x) = \rho V \frac{\partial}{\partial x} [A(x) \, w(x)] \tag{3-57}$$

Where $A(x)$ is the local crossectional area of the body. The rigid body downwash is a function of the angle-of-attack is constant in x,

$$w = V \sin \alpha$$

18

(a) NOSE

CONE

OGIVE

(b) CYLINDRICAL SECTIONS

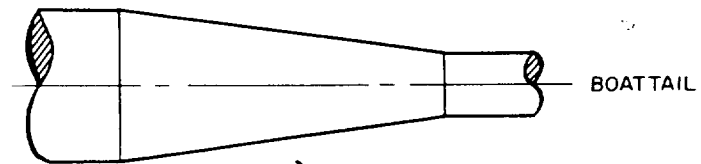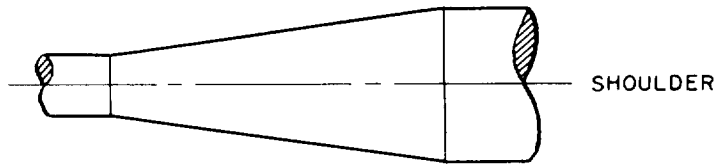(c) CONICAL FRUSTRUMS

SHOULDER

BOATTAIL

Figure 3-7—Body Component Shapes

For angles-of-attack near zero

$$w = V\alpha$$

Then equation 3-57 becomes,

$$n(x) = \rho V^2 \alpha \frac{dA(x)}{dx} \qquad (3\text{-}59)$$

From the definition of normal force coefficient derivative,

$$C_N(x) = \frac{n(x)}{q\,A_r} = \frac{n(x)}{\frac{1}{2}\rho V_0^2\,A_r} \qquad (3\text{-}60)$$

Applying equation 3-60 to 3-59,

$$C_N(x) = \frac{2\alpha}{A_r}\frac{dA(x)}{dx} \qquad (3\text{-}61)$$

Integrating over the length of the body,

$$C_N = \frac{2\alpha}{A_r}\int_0^{l_0}\frac{dA}{dx}dx = \frac{2\alpha}{A_r}\int_0^{l_0}dA \qquad (3\text{-}62)$$

Thus,

$$C_N = \frac{2\alpha}{A_r}\,[A(l_0) - A(0)]^- \qquad (3\text{-}63)$$

By definition of normal force derivative,

$$C_{N_\alpha} = \frac{\partial C_N}{\partial \alpha}\bigg|_{\alpha=0} \qquad (3\text{-}64)$$

equation 3-63 provides,

$$C_{N_\alpha} = \frac{2}{A_r}\,[A(l_0) - A(0)] \qquad (3\text{-}65)$$

Immediately equation 3-65 indicates that C_{N_α} is independent of the body shape as long as the independent of the body shape as long as the integration of equation 3-62 is valid over the body. The

20

body components being analysed are slender and have no discontinuities in their crossectional area or its derivatives. Thus, equation 3-65 may be applied to them. Since the nose tip is assumed to be a sharp point,

$$A(0) = 0$$

Thus, the body normal force coefficient derivative in subsonic flow is;

$$\left(C_{N_\alpha}\right)_B = 2 \frac{A_{BN}}{A_r} \qquad (3\text{-}66)$$

Reference 27 presents a very useful method for determining the normal force coefficient derivative of pointed bodies of revolution in supersonic flow. The second order shock expansion theory approximates the body by a set of tangent conical frustrums. See figure 3-8. The frustrums are each analyzed using an exponential series expansion for the pressure distribution

$$P = -P_0 + C \, e^{(S_0 s + S_1 \frac{s^2}{2} + S_2 \frac{s^3}{3} + \cdots)} \qquad (3\text{-}67)$$

where P_0, C, and S_n are constants for a particular frustrum. By applying the boundary conditions at the leading edge of the frustrum and at infinity while retaining only the first series term the pressure distribution becomes;

$$P = P_e - (P_c - P_2) \, e^{-\eta} \qquad (3\text{-}68)$$

where;

$$\eta = \left(\frac{\partial p}{\partial s}\right)_2 \frac{x - x_2}{(P_c - P_2) \cos \delta_2}$$

s = surface coordinate

P_c = pressure on a cone having the same slope as the frustrum

δ = angle between surface and longitudinal axis

$(\ )_2$ = indicates the value is taken at the front edge of the current frustrum.

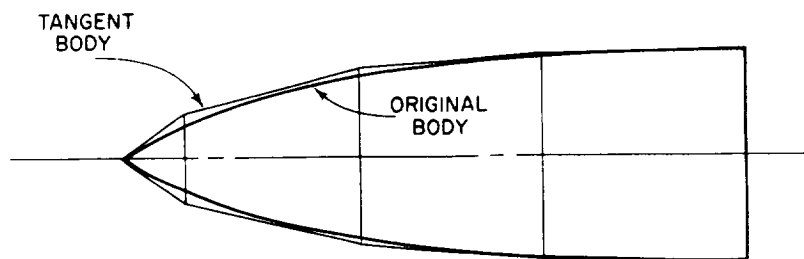21

TANGENT
BODY

ORIGINAL
BODY

Figure 3-8—Approximate Tangent Body

The notation of reference 8 is used and defined to simplify correlation between this presentation and that reference. The value of $(\partial P/\partial s)_2$ is determined by an approximate solution of the generalized characteristic equation in axially symmetric flow,

$$\frac{\partial P}{\partial s} - \lambda \frac{\partial \delta}{\partial s} = \frac{1}{\cos \mu} \frac{\partial P}{\partial C_1} = \frac{-\lambda}{\cos \mu} \left(\frac{\partial \delta}{\partial C_1} + \frac{\sin \mu \sin \delta}{r} \right) \tag{3-69}$$

where

$$\lambda = \frac{2\gamma_p}{\sin 2\mu}$$

C_1 = First Characteristic Coordinate

μ = Mach Angle

r = local radius

γ = ratio of specific heats

The solution is;

$$\left(\frac{\partial P}{\partial s} \right)_2 = \frac{B_2}{r} \left(\frac{\Omega_1}{\Omega_2} \sin \delta_1 - \sin \delta_2 \right) + \frac{B_2}{B_1} \frac{\Omega_1}{\Omega_2} \left(\frac{\partial P}{\partial s} \right)_1 \tag{3-70}$$

where;

$$B = \frac{\gamma_p \cdot M^2}{2(M^2 - 1)}$$

$$\Omega = \frac{1}{M} \left[\frac{1 + \left(\frac{\gamma - 1}{2} \right) M^2}{\frac{\gamma + 1}{2}} \right]^{\frac{\gamma+1}{2(\gamma-1)}} .$$

$(\ )_1$ indicates the value is taken at the trailing edge of the preceeding frustrum.

$(\ )_3$ indicates the value is taken at the trailing edge of the current frustrum.

The value of $(\partial P/\partial s)_1$ is just $(\partial P/\partial s)_3$ of the previous frustrum.

$$\left(\frac{\partial P}{\partial s} \right)_3 = \left(\frac{P_c - P_3}{P_c - P_2} \right) \left(\frac{\partial P}{\partial s} \right)_2 \tag{3-71}$$

By applying equations 3-68, 3-70, and 3-71 to each element in succession, the pressure distribution over the tangent body is determined. The local nondimensional normal load is given by;

$$\Lambda = \frac{n(x)}{\alpha \, \bar{q} \, d} = \frac{2}{\gamma \, M_\infty^2 \, \pi} \int_0^\pi \frac{d(P/P_\infty)}{d\alpha} \cos \phi \, d\phi \qquad (3\text{-}72)$$

where

ϕ = Circumferential Angle.

d = Local diameter.

The derivative of the pressure distribution is evaluated by differentiating equation 3-68 with respect to angle of attack; and then applying physical restraints to simplify the result.

$$\frac{d(P/P_\infty)}{d\alpha} = (1 - e^{-\eta}) \frac{d(P_c/P_\infty)}{d\alpha} + e^{-\eta} \frac{\lambda_2}{\lambda_1} \frac{d(P_1/P_\infty)}{d\alpha} \qquad (3\text{-}73)$$

Using 3-73 in 3-72 and simplifying,

$$\Lambda = (1 - e^{-\eta}) (\tan \delta) \left(C_{N_\alpha} \right)_{tcx} + \frac{\lambda_2}{\lambda_1} e^{-\eta} \Lambda_1 \qquad (3\text{-}74)$$

Where "tcx" indicates the value of an equivalent cone. The running load distribution is determined by successive application of equation 3-74 to the tangent body elements. The value of Λ_1, for the initial cone is just,

$$\Lambda_1 = (\tan \delta_v) \left(C_{N_\alpha} \right)_{tcv} \qquad (3\text{-}75)$$

Where "v" and "tcv" are the values at the initial equivalent cone vertex. The normal force coefficient derivative is determined by the longitudinal integration of the running load distribution.

$$\left(C_{N_\gamma} \right)_B = \frac{2\pi}{A_B} \int_0^1 \Lambda \, r \, dx \qquad (3\text{-}76)$$

where;

A_B = Body Base Area.

1 = Body Length.

The initial cone and equivalent cone characteristics are obtained from references 24 and 25; and are presented in tables 3-1 thru 3-3.

Table 3-1—Values of M at Initial Cone Surface

M	2.5	5.0	7.5	10.0	12.5	15.0	17.5	20.0	22.5	25.0	27.5	30.0
1.5	1.4866884	1.4579318	1.4197316	1.3748579	1.3248992	1.2707392	1.2127162	1.1506488	1.0837313	1.0100703		
1.75	1.7340335	1.7004643	1.6568043	1.6064462	1.5513276	1.4925484	1.4306418	1.3657361	1.2976505	1.2259024	1.1495789	1.0669388
2.0	1.9808615	1.9415254	1.8912335	1.8340453	1.7721933	1.7068837	1.6386764	1.5677572	1.4940884	1.4174680	1.3375202	1.2535953
2.5	2.4729472	2.4193976	2.3528628	2.2788768	2.2001554	2.1179422	2.0327606	1.9448503	1.8543543	1.7613748	1.6659616	1.5680718
3.0	2.9627600	2.8913832	2.8048038	2.7101402	2.6103929	2.5067511	2.3997895	2.2899646	2.1777409	2.0635830	1.9479054	1.8310067
3.5	3.4500939	3.3571597	3.2467499	3.1275136	3.0025569	2.8731152	2.7400668	2.6043443	2.4669130	2.3286833	2.1904152	2.0526629
4.0	3.9347700	3.8164543	3.6783916	3.5305680	3.3761469	3.2166972	3.0537628	2.8889908	2.7239783	2.5600783	2.3983186	2.2393739
4.5	4.4166246	4.2690580	4.0994611	3.9189007	3.7307750	3.5374323	3.3414321	3.1453333	2.9513677	2.7612386	2.5760876	2.3965344
5.0	4.8955305	4.7148078	4.5097079	4.2921847	4.0662668	3.8355932	3.6040616	3.3752078	3.1517935	2.9356870	2.7279347	2.5289133
6.0	5.8440686	5.5852474	5.2968787	4.9927832	4.6801702	4.3668118	4.0597311	3.7640785	3.4829712	3.2178167	2.9687934	2.7352580
7.0	6.7796857	6.4269172	6.0384888	5.6318010	5.2204850	4.8178049	4.4335119	4.0731395	3.7388047	3.4303400	3.1462500	2.8843548
8.0	7.7018785	7.2390804	6.7337145	6.2103924	5.6922672	5.1981506	4.7389543	4.3187765	3.9373126	3.5918831	3.2787858	2.9940481
10.0	9.5046400	8.7725147	7.9851813	7.1977580	6.4568340	5.7867581	5.1933727	4.6723717	4.2153623	3.8131019	3.4569163	3.1391940
12.0	11.250395	10.182053	9.0582962	7.9858490	7.0291308	6.2043028	5.5019835	4.9042678	4.3926921	3.9510537	3.5659952	3.2267626
15.0	13.759139	12.063489	10.368285	8.8727901	7.6324201	6.6228697	5.7997803	5.1216448	4.5552592	4.0753516	3.6629457	3.3037471
20.0	17.637850	14.613515	11.919518	9.8177450	8.2281047	7.0145241	6.0679293	5.3119812	4.6946790	4.1802823	3.7437969	3.3673365

Table 3-2–Values of $\left(\dfrac{dC_N}{d\alpha}\right)_{\alpha=0}$ for Equivalent Cones

M \ δ	2.5	5.0	7.5	10.0	12.5	15.0	17.5	20.0	22.5	25.0	27.5	30.0
1.5	1.9770483	1.9336127	1.8821566	1.8280992	1.7735619	1.7187816	1.6630926	1.6057182	1.5462941	1.4852936		
1.75	1.9731742	1.9258447	1.8737533	1.8224578	1.7730646	1.7243971	1.6746400	1.6223425	1.5666956	1.5075064	1.4451701	1.3808820
2.0	1.9690287	1.9180672	1.8661051	1.8183423	1.7742540	1.7310117	1.6859216	1.6372641	1.5842135	1.5265736	1.4645815	1.3988695
2.5	1.9602967	1.9036740	1.8548454	1.8161039	1.7820973	1.7472553	1.7083329	1.6638860	1.6134668	1.5571606	1.4953496	1.4286279
3.0	1.9514206	1.8917127	1.8493550	1.8202950	1.7941549	1.7645092	1.7287097	1.6859461	1.6362061	1.5798551	1.5174588	1.4497109
3.5	1.9426977	1.8826075	1.8487600	1.8282076	1.8074148	1.7806466	1.7461812	1.7037859	1.6537994	1.5968132	1.5335317	1.4647351
4.0	1.9343213	1.8763907	1.8516843	1.8377630	1.8203259	1.7949749	1.7608321	1.7181330	1.6674853	1.6096523	1.5454397	1.4756774
4.5	1.9264473	1.8728601	1.8568202	1.8477350	1.8322685	1.8074272	1.7730368	1.7296967	1.6782310	1.6195188	1.5544309	1.4838272
5.0	1.9191785	1.8715909	1.8632046	1.8574765	1.8430453	1.8181556	1.7832011	1.7390731	1.6867491	1.6272149	1.5613461	1.4900257
6.0	1.9066985	1.8741557	1.8772933	1.8752450	1.8611884	1.8352940	1.7988073	1.7530357	1.6991506	1.6381839	1.5710540	1.4986224
7.0	1.8972025	1.8808308	1.8911403	1.8902959	1.8754007	1.8479983	1.8098978	1.7626404	1.7074620	1.6453960	1.5773421	1.5041237
8.0	1.8906735	1.8893943	1.9037986	1.9027991	1.8865235	1.8575153	1.8179511	1.7694507	1.7132534	1.6503536	1.5816157	1.5078364
10.0	1.8854155	1.9075860	1.9248544	1.9216225	1.9022129	1.8703588	1.8284727	1.7781460	1.7205191	1.6564935	1.5868584	1.5123524
12.0	1.8876297	1.9243231	1.9408134	1.9345246	1.9122898	1.8782443	1.8347389	1.7832191	1.7246910	1.6599792	1.5898124	1.5148790
15.0	1.8980460	1.9449893	1.9576949	1.9470431	1.9215589	1.8852675	1.8402027	1.7875704	1.7282369	1.6629184	1.5922831	1.5169846
20.0	1.9201707	1.9690214	1.9743436	1.9583547	1.9295376	1.8911343	1.8446777	1.7910947	1.7310758	1.6652577	1.5942431	1.5186494

Table 3-3—Values of Surface Pressure Coefficient for Equivalent Cones

M\δ	2.5	5.0	7.5	10.0	12.5	15.0	17.5	20.0	22.5	25.0	27.5	30.0
1.5	.0123382	.0396615	.0773864	.1237983	.1781167	.2400313	.3095450	.3869791	.4731538	.5699888		
1.75	.0114414	.0363287	.0704289	.1122701	.1612014	.2169225	.2792900	.3482459	.4238192	.50619022	.59585744	.69405243
2.0	.0107862	.0339457	.0655812	.1044583	.1500854	.2022339	.2607607	.3255312	.39641336	.47330179	.55616008	.64511954
2.5	.00982981	.03058576	.05895952	.09413081	.1358608	.1840343	.23852578	.29915906	.36571047	.43791904	.51550425	.59818912
3.0	.00913541	.02824024	.05451919	.08747518	.1270239	.17310135	.22558051	.28426241	.34888446	.41912862	.49463659	.57503078
3.5	.00859242	.02647476	.05130225	.08281755	.12101992	.16585924	.21719882	.27481810	.33842506	.40766937	.48215440	.56145326
4.0	.00814929	.02508810	.04886536	.07939344	.11671212	.16077021	.21141454	.26840424	.33142494	.40010296	.47401780	.55271448
4.5	.00777855	.02396847	.04696202	.07678924	.11350386	.15704447	.20724252	.26383657	.32649601	.39482976	.46839852	.54673311
5.0	.00746199	.02304657	.04544267	.07475691	.11104466	.15423167	.20413070	.26046646	.32289183	.39100288	.46435008	.54245194
6.0	.00694671	.02162337	.04318936	.07182851	.10757999	.15033841	.19988673	.25592332	.31807966	.38593639	.45902778	.53685790
7.0	.00654427	.02058479	.04162143	.06985826	.10530922	.14783838	.19720408	.25308627	.31510472	.38282933	.45578647	.53347449
8.0	.00622092	.01980211	.04048580	.06847199	.10374427	.14614133	.19540407	.25120009	.31314047	.38078911	.45366854	.53127090
10.0	.00573592	.01871810	.03898810	.06670277	.10179238	.14406008	.19322118	.24893118	.31079304	.37836321	.45115963	.52867228
12.0	.00539243	.01802077	.03807635	.06566456	.10067415	.14288515	.19200207	.24767463	.30949966	.37703244	.44978975	.52725561
15.0	.00503756	.01736467	.03726273	.06476571	.09972302	.14189705	.19098631	.24663061	.30843098	.37593703	.44866381	.52609497
20.0	.00468137	.01677876	.03657736	.06403097	.09895953	.14111270	.19018534	.24581285	.30759370	.37507865	.44778536	.52519347

3.22 BODY CENTER OF PRESSURE LOCATION

As in the subsonic body normal force coefficient derivative analysis, it is required that there be no discontinuities between the body component shapes in order to allow integration over the entire body.

By definition, the pitching moment of the local aerodynamic force about the front of the body $(x = 0)$ is;

$$\overline{m}(x) = xn(x) \tag{3-77}$$

The pitch moment coefficient is defined as;

$$C_m = \frac{\overline{m}}{q A_r L_r} \tag{3-78}$$

thus,

$$C_m = \frac{xn(x)}{q A_r L_r} \tag{3-79}$$

Since,

$$C_N = \frac{n}{q A_r} \tag{3-80}$$

equation (3-79) becomes

$$C_m(x) = \frac{x C_N(x)}{L_r} \tag{3-81}$$

The value of the subsonic local normal force coefficient is given in equation 3-61. Using it in equation 3-81.

$$C_m(x) = \frac{2 \alpha x}{A_r L_r} \frac{dA(x)}{dx} \tag{3-82}$$

Integrating over the length of the body,

$$C_m = \frac{2 \alpha}{A_r L_r} \int_0^{l_0} x \left(\frac{dA(x)}{dx} \right) dx \tag{3-83}$$

28

This can be integrated by parts;

$$u = x \qquad dv = \left(\frac{dA(x)}{dx}\right) dx$$

$$du = dx \qquad v = A(x)$$

giving;

$$C_m = \frac{2\alpha}{A_r L_r} \left[l_0 A(l_0) - \int_0^{l_0} A(x)\, dx \right] \tag{3-84}$$

But, by definition, the integral term is the body volume, therefore;

$$C_m = \frac{2\alpha}{A_r L_r} \left[l_0 A(l_0) - V_B \right] \tag{3-85}$$

By definition, the pitch moment coefficient derivative is;

$$C_{m_\alpha} = \frac{\partial C_m}{\partial \alpha}\bigg|_{\alpha=0} \tag{3-86}$$

Then; from equation 3-85,

$$\left(C_{m_\alpha}\right)_B = \frac{2}{A_r L_r} \left[l_0 A(l_0) - V_B \right] \tag{3-87}$$

The center of pressure is determined by,

$$\bar{X}_B = \frac{\left(C_{m_\alpha}\right)_B}{\left(C_{N_\alpha}\right)_B} L_r \tag{3-88}$$

Using equations 3-65 and 3-87 in 3-88 and simplifying yields,

$$\bar{X}_B = l_0 - \frac{V_B}{A_B} \tag{3-89}$$

29

The volume formulae for cones, conical frustrums and circular cylinders are well known and do not merit repetition in this paper. However, the volume formula for a tangent ogive is not readily available and is given herein for the readers convenience. The volume of a tangent ogive nose shape is determined in reference 12 as;

$$\frac{(V_B)_{ogive}}{d_N\, A(L)} = f_N \left(f_N^2 + \frac{1}{4}\right)^2 - \frac{1}{3} f_N^3 - \left(f_N^2 - \frac{1}{4}\right)\left(f_N^2 + \frac{1}{4}\right)^2 \sin^{-1}\left(\frac{f_N}{f_N^2 + \frac{1}{4}}\right) \tag{3-90}$$

where;

$$f_N = \frac{L_N}{d_N}$$

In supersonic flow, the method of reference 27 determines the pitch moment coefficient derivative as,

$$C_{m_\alpha} = \frac{-2\pi}{A_B\, d} \int_0^{\ell} \Lambda\, r x\, dx \tag{3-91}$$

Where $\Lambda(x)$ is found using equation 3-74. The center of pressure location of the body in supersonic flow is then determined by the use of equations 3-76 and 3-91 in equation 3-88,

$$\bar{X}_B = \left(\frac{C_{m_\alpha}}{C_{N_\alpha}}\right) d \tag{3-92}$$

3.30 TAIL-BODY INTERFERENCE EFFECTS

The effect of interference flow between the tail and the body on the normal force aerodynamics of a slender, finned vehicle can be expressed in terms of interference factors (reference 23).

$$\left(C_{N_\alpha}\right)_{T(B)} = \left(C_{N_\alpha}\right)_T K_{T(B)} \tag{3-93}$$

$$\left(C_{N_\alpha}\right)_{B(T)} = \left(C_{N_\alpha}\right)_T K_{B(T)} \tag{3-94}$$

$$\left(C_{\ell_\delta}\right)_{T(B)} = \left(C_{\ell_\delta}\right)_T k_{T(B)} \tag{3-95}$$

The interference factors are determined by applying slender body theory to the flow over the total vehicle.

3.31 TAIL IN THE PRESENCE OF THE BODY

Because the fins under consideration are of low aspect ratio, the value of $K_{T(B)}$ is available from references 7 and 17.

$$K_{T(B)} = \frac{2}{\pi \left(1 - \frac{1}{\tau}\right)^2} \left\{ \left(1 + \frac{1}{\tau^4}\right)\left[\frac{1}{2}\tan^{-1}\frac{1}{2}\left(\tau - \frac{1}{\tau}\right)\right] - \frac{1}{\tau^2}\left[\left(\tau - \frac{1}{\tau}\right) + 2\tan^{-1}\left(\frac{1}{\tau}\right)\right] \right\} \qquad (3\text{-}96)$$

Reference 23 determines that the longitudinal tail center-of-pressure is independent of the interference flow.

$$\bar{X}_{T(B)} = \bar{X}_T \qquad (3\text{-}97)$$

3.32 BODY IN THE PRESENCE OF THE TAIL

The only portion of the body affected by interference flow is the portion between and behind the fins. Subsonically, slender body theory, reference 3, determines;

$$K_{B(T)} = \frac{\left(1 - \frac{1}{\tau^2}\right)^2}{\left(1 - \frac{1}{\tau}\right)^2} - K_{T(B)} \qquad (3\text{-}98)$$

where $K_{T(B)}$ is given by equation 3-96. In supersonic flow, the interference effect on the body can be strongly affected by the fin tip mach cone. The fin tip mach cone intersects the body when,

$$\beta \, R \, (1 + \lambda) \left(\frac{1}{\beta m} + 1\right) > 4 \qquad (3\text{-}99)$$

Until this condition is reached equation 3-98 is still valid in supersonic flow. Once the fin tip mach cone impinges on the body, the function becomes quite complex and is more easily presented in the form of curves. Figure 3-9 shows the variation of the corrected interference factor. Using the result of this curve, $K'_{B(T)}$;

31

$$\left(C_N\right)_{B(T)} = K'_{B(T)} \,(1 \cdots) \,(\tau - 1) \tag{3-100}$$

By the extension of the fin lifting line into the body, reference 23 derives the subsonic variation of the center-of-pressure location of the tail interference flow over the body.

$$\bar{X}_{B(T)} = l_T + \frac{c_r}{4} + \left[\frac{\sqrt{s^2 - r_t^2}\, \cosh^{-1}\left(\frac{s}{r_t}\right) - s + \frac{\pi}{2}\, r_t}{\dfrac{r_t}{\sqrt{s^2 - r_t^2}}\, \cosh^{-1}\left(\frac{s}{r_t}\right) + \frac{s}{r_t} - \frac{\pi}{2}} - r_t \right] \tan \Gamma_{1/4} \tag{3-101}$$

Where, $s > r$ and $\beta\!R \geq 4$. In addition, slender body theory is applied subsonically to find $\bar{X}_{B(T)}$ at $\beta\!R = 0$. Slender body $\bar{X}_{B(T)}$ values are obtained at intermediate $\beta\!R$ values only for $\lambda = 1$. For other values of λ and sweep the $\bar{Y}_{B(T)}$ curves are interpolated between the lifting line values and the slender body value at $\beta\!R = 0$. The shape of the interpolated curves is assumed similar to the $\lambda = 1$ curve. Figure 3-10 shows the full subsonic $\bar{X}_{B(T)}$ variation. In supersonic flow, the center-of-pressure of the interference flow over the body is found by applying equation 3-92;

$$\bar{X}_{B(T)} = \frac{\left(C_{m_\alpha}\right)_{B(T)}}{\left(C_{N_\alpha}\right)_{B(T)}}\, d + l_T \tag{3-102}$$

Reference 23 gives the body interference pitch moment derivative as derived from slender body theory;

$$\left(C_{m_\alpha}\right)_{B(T)} = -\frac{8(m\beta)^{3/2}}{A_r\,\pi\beta\,(\beta_m + 1)} \int_0^d dy \int_{\beta y}^{C_r} x \cos^{-1}\left(\frac{\frac{x}{\beta} - \beta my}{mx - y}\right) dx \tag{3-103}$$

This is for fins with supersonic leading edges, $m\beta > 1$. For subsonic leading edges, $m\beta < 1$ and,

$$\left(C_{m_\alpha}\right)_{B(T)} = -\frac{4\beta m}{A_r\,\pi\beta\,\sqrt{\beta^2 m^2 - 1}} \int_0^d dy \int_{\beta y}^{C_r} \frac{x\sqrt{\frac{x}{\beta} + y}}{\sqrt{mx - y}} dx \tag{3-104}$$

32

The vertical axis is labeled:

$$K'_{B(T)} = K_{B(T)} (\beta C_{N_\alpha})_T (\lambda_T + 1)(\frac{s_T}{r_T} - 1)$$

The horizontal axis is labeled:

$$\frac{2\beta_{r_T}}{(C_r)_T}$$

Curves labeled βm_T: ∞, 4, 2, 1, 0.8, 0.6, 0.4, 0.2

Text on graph:
$$(\beta A)(1+\lambda)(\frac{1}{m\beta}+1) > 4$$
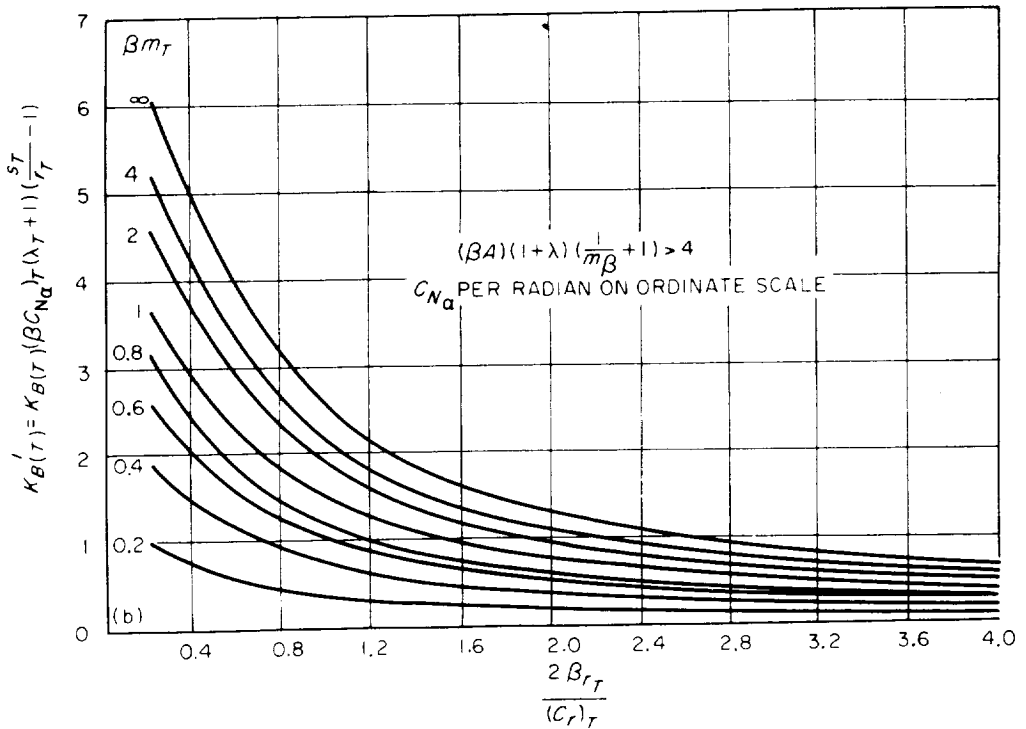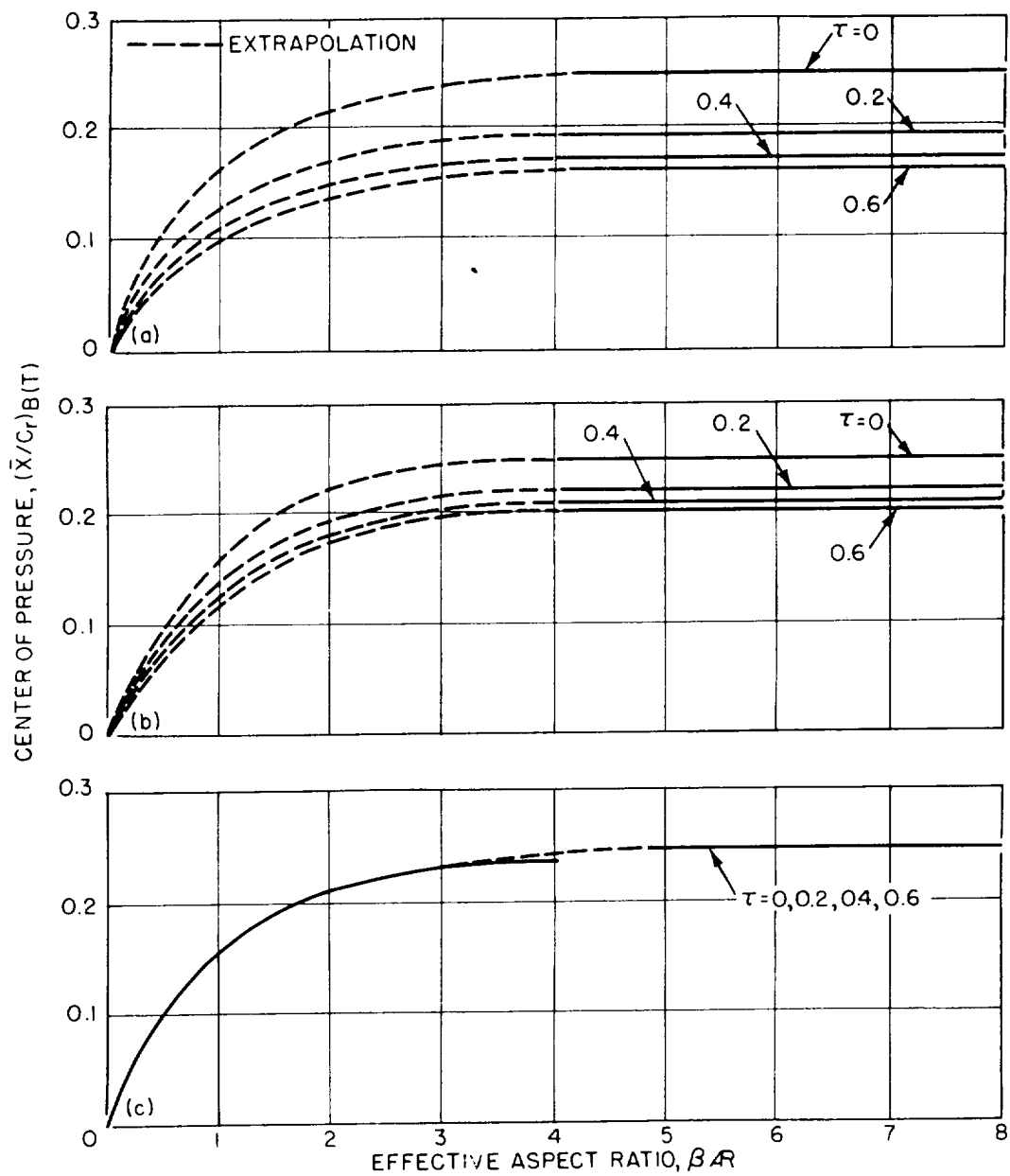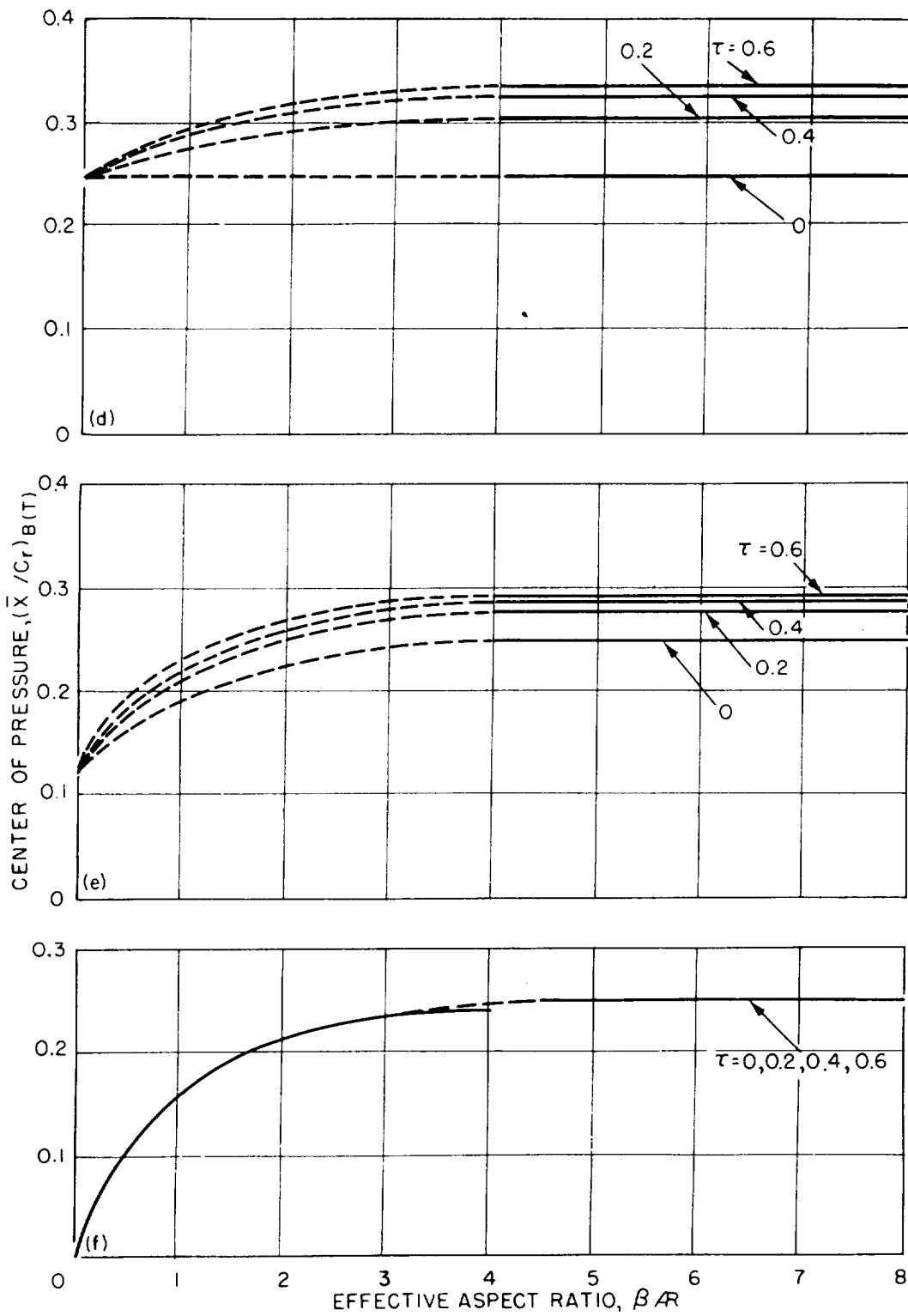C_{N_α} PER RADIAN ON ORDINATE SCALE

(b)

Figure 3-9—Supersonic $K_{B(T)}$

33

a) NO LEADING-EDGE SWEEP, $\lambda = 0$. (b) NO LEADING-EDGE SWEEP, $\lambda = \frac{1}{2}$ (c) NO LEADING-EDGE SWEEP, $\lambda = 1$.

Figure 3-10—Subsonic $\bar{X}_{B(T)}$

34

(d) NO MIDCHORD SWEEP, $\lambda = 0$. (e) NO MIDCHORD SWEEP, $\lambda = \frac{1}{2}$. (f) NO MIDCHORD SWEEP, $\lambda = 1$.

Figure 3-10 (Continued)—Subsonic $\overline{X}_{B(T)}$

35
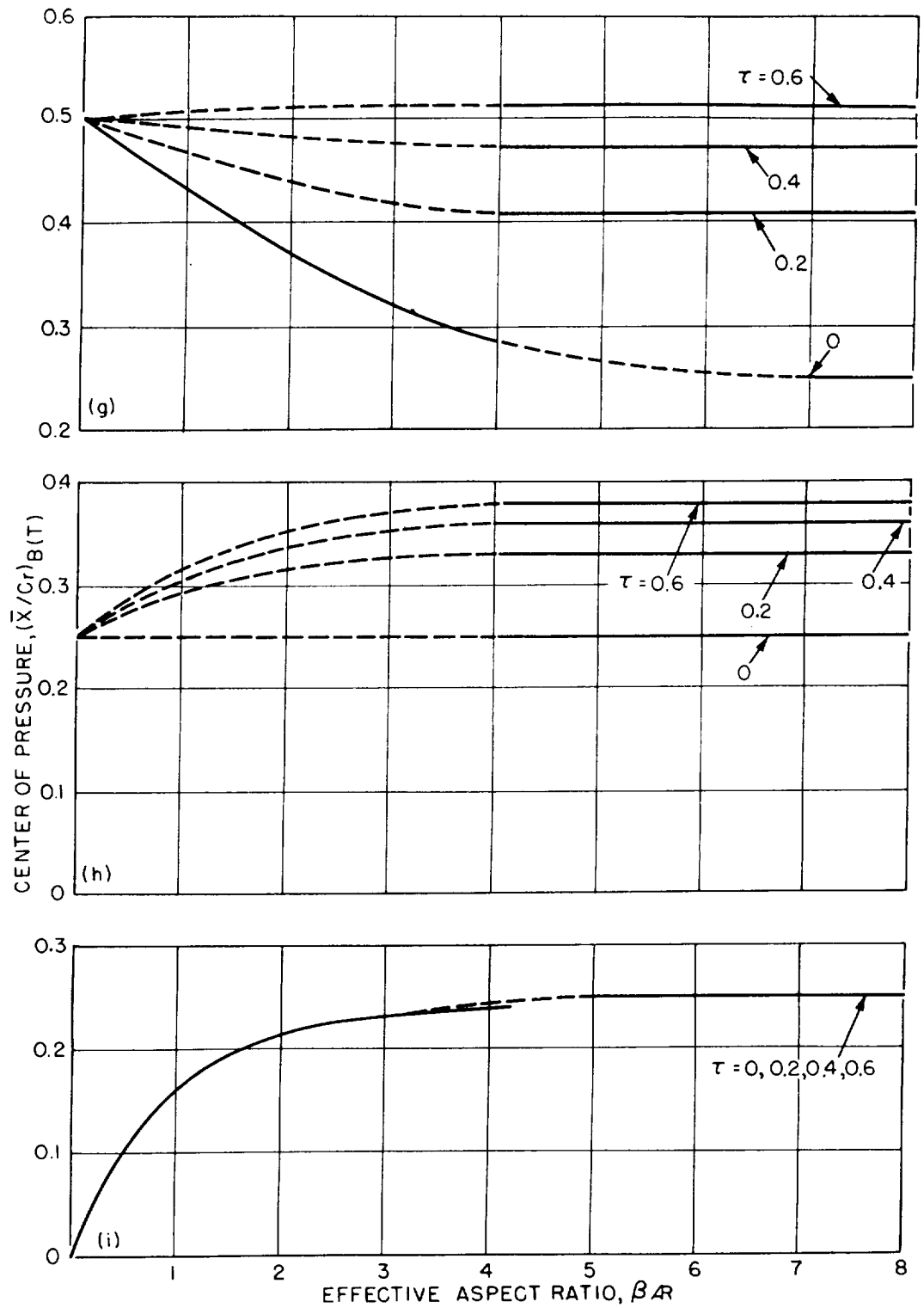
(g) NO TRAILING-EDGE SWEEP, $\lambda=0$. (h) NO TRAILING-EDGE SWEEP, $\lambda=\frac{1}{2}$. (i) NO TRAILING EDGE SWEEP, $\lambda=1$.

Figure 3-10 (Continued)—Subsonic $\overline{X}_{B(T)}$

Where the coordinate system has been given in figure 3-2. $\overline{X}_{B(T)}$ is determined by using equation 3-100 along with either 3-103 or 3-104 in equation 3-102. The result is shown in figure 3-11.

3.33 CANTED TAIL IN THE PRESENCE OF THE BODY

The effect of fin cant at zero angle-of-attack is determined in a manner similar to the effect at an angle-of-attack alone. Reference 23 determines the corresponding interference factor,

$$
\begin{aligned}
k_{T(B)} = \frac{1}{\pi^2} \Bigg[& \frac{\pi^2}{4} \frac{(\tau+1)^2}{\tau^2} + \frac{\pi(\tau^2+1)^2}{\tau^2(\tau-1)^2} \sin^{-1}\left(\frac{\tau^2-1}{\tau^2+1}\right) - \frac{2\pi(\tau+1)}{\tau(\tau-1)} \\
& + \frac{(\tau^2+1)^2}{\tau^2(\tau-1)^2}\left(\sin^{-1}\frac{\tau^2-1}{\tau^2+1}\right)^2 - \frac{4(\tau+1)}{\tau(\tau-1)} \sin^{-1}\left(\frac{\tau^2-1}{\tau^2+1}\right) \\
& + \frac{8}{(\tau-1)^2} \ln\left(\frac{\tau^2+1}{2\tau}\right) \Bigg]
\end{aligned}
\tag{3-105}
$$

No center of pressure value need be considered for the canted fin in the presence of the body since only the roll moment derivative is considered.

3.40 TOTAL NORMAL FORCE AERODYNAMICS

The total normal force coefficient derivative is the sum of all the components.

$$
C_{N_\alpha} = \left(C_{N_\alpha}\right)_B + \left(C_{N_\alpha}\right)_{T(B)} + \left(C_{N_\alpha}\right)_{B(T)}
\tag{3-106}
$$

The overall center of pressure is the solution of the moment sum of the components.

$$
\overline{X} = \frac{\overline{X}_B \left(C_{N_\alpha}\right)_B + \overline{X}_{T(B)} \left(C_{N_\alpha}\right)_{T(B)} + \overline{X}_{B(T)} \left(C_{N_\alpha}\right)_{B(T)}}{C_{N_\alpha}}
\tag{3-107}
$$

The value of total $\overline{Y}$ is zero. The total C_{ℓ_s} value is determined from equation 3-95.

3.41 PITCH DAMPING MOMENT COEFFICIENT DERIVATIVE

When the vehicle has an angular pitch velocity, the superposition of the local pitch velocity at the fins on the free stream velocity produces a local angle of attack which is constant across the fins. See figure 3-12. The moment produced by the induced force is;
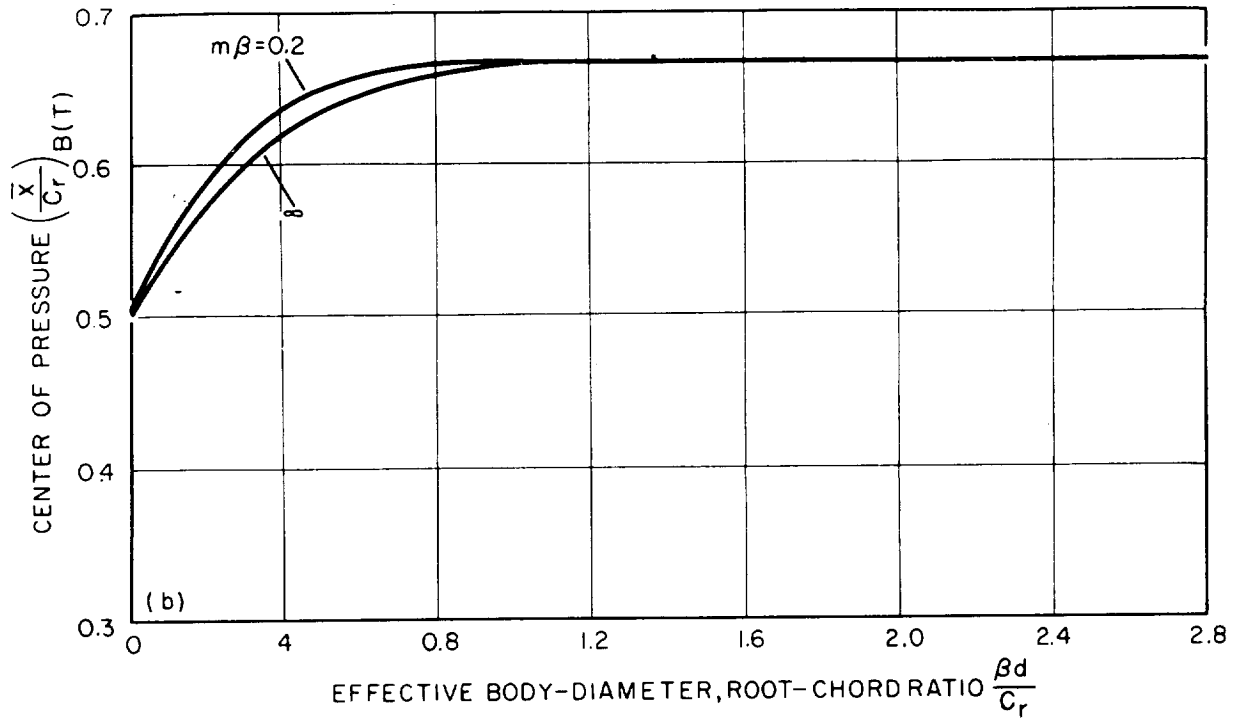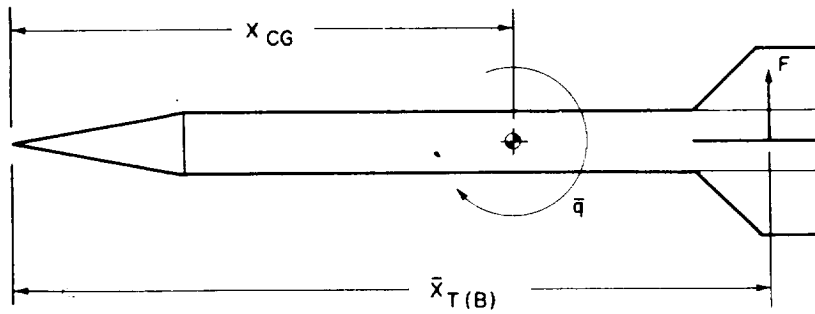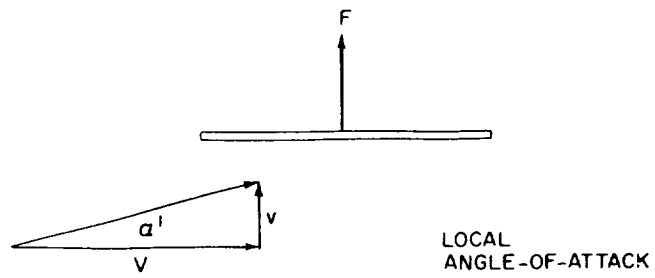
Figure 3-11—Supersonic $\overline{X}_{B(T)}$

OVERALL PARAMETERS

LOCAL
ANGLE-OF-ATTACK

Figure 3-12—Pitch Damping Parameters

$$\bar{m} = F(\Delta x) \tag{3-108}$$

where;

$$\Delta x = \bar{X}_{T(B)} - X_{CG}$$

But,

$$F = \left(C_N \right)_{T(B)} \alpha' A_r \bar{q} \tag{3-109}$$

and,

$$\alpha' = \tan^{-1} \left(\frac{v}{V} \right)$$

For $V \gg v$,

$$\alpha' = \frac{v}{V} \tag{3-110}$$

the local pitch velocity is,

$$v = q(\Delta x) \tag{3-111}$$

Combining equation 3-108, 3-109, 3-110, and 3-111 and simplifying;

$$\bar{m} = \left(C_{N_\alpha} \right)_{T(B)} (\Delta X)^2 A_r \bar{q} \left(\frac{q}{V} \right) \tag{3-112}$$

Knowing the definition of pitch moment coefficient, equation 3-78,

$$C_m = \left(C_{N_\alpha} \right)_{T(B)} \frac{(\Delta x)^2}{L_r} \left(\frac{q}{V} \right) \tag{3-113}$$

The pitch damping moment coefficient derivative is defined as,

$$C_{mq} = \left. \frac{\partial C_m}{\partial \left(\frac{qL_r}{2V} \right)} \right|_{\frac{qL_r}{2V} = 0} \tag{3-114}$$

Thus, using equation 3-113 in 3-114.

Equation 3-123 is equally applicable to three and four fin configurations since the tail normal force derivative is corrected for dihedral effects.

3.42 ROLL DAMPING IN THE PRESENCE OF THE BODY

Any tail body interference factor may be expressed as the ratio,

$$K = \frac{\int_r^{s+r} \alpha_i(\xi)\, c(\xi)\, d\xi}{\int_r^{s+r} \alpha_0(\xi)\, c(\xi)\, d\xi} \tag{3-116}$$

(See figure 6) where;

$\alpha_i(\xi)$ = the angle-of-attack variation over the fin in the presence of the body

$\alpha_0(\xi)$ = the angle-of-attack variation over the fin alone.

Reference 23 gives the value of $\alpha_i(\xi)$ for a tail-body combination at an angle of attack, α, as;

$$\alpha_i(\xi) = \alpha + \frac{r^2}{\xi^2}\, \alpha_B \tag{3-117}$$

where α_B is the angle of attack at the body surface. For the case of the tail-body combination at an angle of attack,

$$\alpha_B = \alpha = \alpha_0(\xi)$$

However, for a rolling vehicle at a zero angle of attack, equation 3-39 gives;

$$\alpha_0(\xi) = -\frac{P\xi}{V}$$

and

$$\alpha_B = -\frac{Pr}{V} \tag{3-118}$$

Then, equations 3-39, 3-117, and 3-118 give,

$$\alpha_i(\xi) = -\frac{P}{V}\left(\xi + \frac{r^3}{\xi^2}\right) \tag{3-119}$$

Therefore, the roll damping interference factor, $k_{R(B)}$, becomes

$$k_{R(B)} = \frac{\int_r^{s+r} -\frac{P}{V}\left(\xi + \frac{r^3}{\xi^2}\right) c(\xi)\, d\xi}{\int_r^{s+r} -\frac{P}{V} \xi\, c(\xi)\, d\xi} \tag{3-120}$$

Simplifying;

$$k_{R(B)} = 1 + \frac{\int_r^{s+r} \frac{c(\xi)}{\xi^2}\, d\xi}{\int_r^{s+r} \xi\, c(\xi)\, d\xi} \tag{3-121}$$

Integrating equation 3-121 using the chord variation given by equation 3-42 yields,

$$k_{R(B)} = 1 + \frac{\dfrac{\tau - \lambda}{\tau} - \dfrac{1 - \lambda}{\tau - 1}\ln \tau}{\dfrac{(\tau + 1)(\tau - \lambda)}{2} - \dfrac{(1 - \lambda)(\tau^3 - 1)}{3(\tau - 1)}} \tag{3-122}$$

The roll damping moment coefficient derivative can then be expressed as,

$$\left(C_{\ell_p}\right)_{T(B)} = \left(C_{\ell_p}\right) k_{R(B)} \tag{3-123}$$

Where $k_{R(B)}$ is given by equation 3-122.

4.00 AXIAL FORCE AERODYNAMICS

The only coefficient dependent on the aerodynamic forces acting parallel to the longitudinal axis of the vehicle is the drag coefficient. Drag forces arise from two basic mechanisms, skin friction and pressure distribution. Since both mechanisms, and their interactions, are extremely

complex, most practical theoretical drag computations must be tempered with statistical and empirical data. The majority of the equations derived in this section are either theoretical generalizations of statistical-empirical data or direct curve fits of experimental results.

4.10 SKIN FRICTION DRAG

The skin friction coefficient is defined as the skin friction drag of a plane surface divided by the dynamic pressure and the wetted area of the surface.

$$C_f = \frac{D_{friction}}{\bar{q} \, A_w} \tag{4-1}$$

4.11 INCOMPRESSIBLE FLOW SKIN FRICTION COEFFICIENT

The skin friction coefficient for incompressible flow can be expressed in terms of the reynolds number, see figure 4-1. For laminar flow, their relation has been established both experimentally and by theoretical boundary layer considerations, reference 6.

$$C_f = \frac{1.328}{\sqrt{R_e}} \tag{4-2}$$

For reynolds numbers greater than about 5×10^5 the boundary layer flow becomes transitional and then turbulent. No good theoretical solutions have been found for turbulent flow. Figure 4-1 shows the experimental data for turbulent skin friction. Schoenherr applied the theoretical boundary layer work of von Karman to the experimental data and established the turbulent flow relationship;

$$\log (R_e \, C_f) = \frac{0.242}{\sqrt{C_f}} \tag{4-3}$$

Hama formed a simpler formula which agrees with equation 4-3 within ±2%.

$$C_f = \frac{1}{(3.46 \log R_e - 5.6)^2} \tag{4-4}$$

The form of the transitional curve may be approximated by subtracting an increment from equation 4.4. The increment has the form

$$\Delta C_f = \frac{k}{R_e} \tag{4-5}$$

Based on experimental data Prandtl indicated that $k = 1700$. This fact, as well as other possible transitional curves are shown on figure 4-1. Combining equations 4-4 and 4-5,
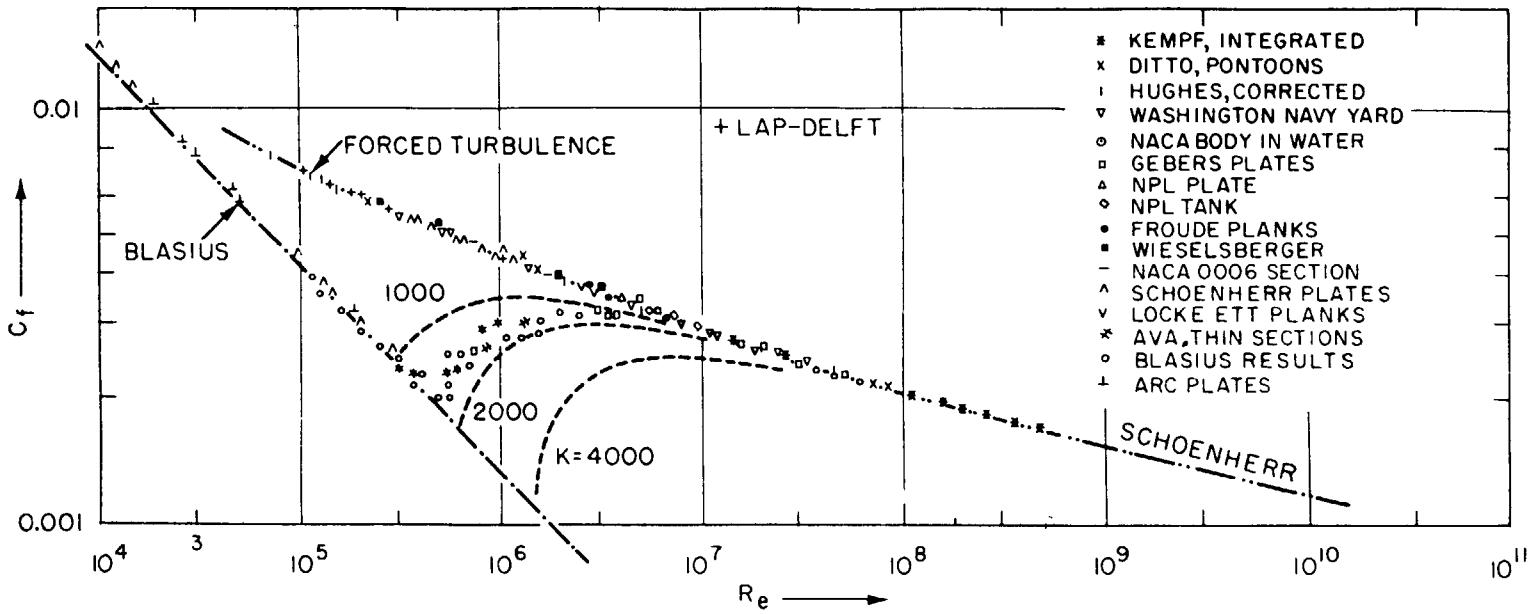
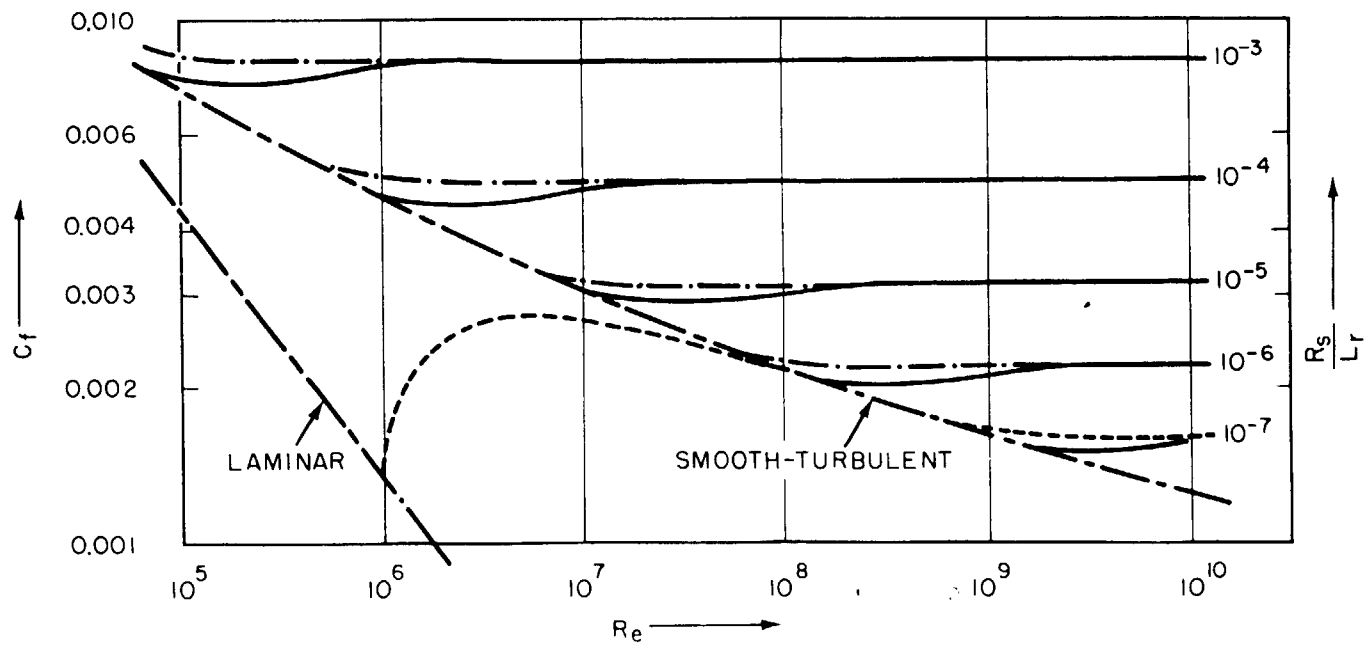Figure 4-1—Skin Friction Coefficient

44

Figure 4-2—Skin Friction With Roughness

45

Table 4-1
Approximate Surface Roughness Heights of
Physical Surfaces

Type of Surface	Approximate microns	R_S in mils
Surfaces like that of a "mirror"	0	0
Surface of average glass	0.1	0.004
Finished and polished surfaces	0.5	0.02
Aircraft-type sheet-metal surfaces	2	0.1
Optimum paint-sprayed surfaces	5	0.2
Planed wooden boards	15	0.6
Paint in aircraft-mass production	20	1
Steel plating – bare	50	2
Smooth cement surface	50	2
Surface with asphalt-type coating	100	4
Dip-galvanized metal surface	150	6
Incorrectly sprayed aircraft paint	200	8
Natural surface of cast iron	250	10
Raw wooden boards	500	20
Average concrete surface	1000	40

$$C_f = \frac{1}{(3.46 \log R_e - 5.6)^2} - \frac{1700}{R_e} \qquad (4\text{-}6)$$

for $R_e > 5 \times 10^5$.

The above considerations are for surface roughness sizes that are submerged in the laminar sublayer. For appreciable rough surfaces the turbulent skin friction coefficient is shown in figure 4-2. The "smooth" curve is followed until the critical reynolds number corresponding to the roughness is reached.

$$(R_e)_{cr} = 51 \left(\frac{R_s}{L_r}\right)^{-1.039} \qquad (4\text{-}7)$$

For reynolds numbers higher than the critical value, the skin friction coefficient can be considered independent of reynolds number, reference 6.

$$C_f = 0.032 \left(\frac{R_s}{L_r}\right)^{.2} \qquad (4\text{-}8)$$

The flow is considered to be turbulent throughout the reynolds number range since the roughness trips transition even at low reynolds numbers. Table 4-1 is a list from reference 6 of the approximate average roughness heights for physical surfaces.

4.12 COMPRESSIBLE SUBSONIC VARIATION

In compressible subsonic flow reference 6 indicates that the laminar skin friction coefficient remains unchanged while the "smooth" turbulent value varies as,

$$C_{f_c} = C_f (1 - .09 \, M^2) \qquad (4\text{-}9)$$

and the change for turbulent flow with roughness is,

$$C_{f_c} = C_f (1 - .12 \, M^2) \qquad (4\text{-}10)$$

4.13 SUPERSONIC VARIATION

Theoretical solutions in reference 16 indicate that the supersonic variation of the Laminar skin friction coefficient is;

$$C_{f_c} = \frac{C_f}{(1 + .045 \, M^2)^{1/4}} \qquad (4\text{-}11)$$

This has been confirmed by experimental data, reference 6. Experimental data, reference 6, for the variation of "smooth" turbulent C_{f_c} in supersonic flow indicates a strong dependence on the wall

heat transfer as well as mach number, figure 4-3. The wall temperature alternatives shown are the two possible extremes. The actual condition would probably be closest to the recovery temperature. The curve fit of figure 4-3 is,

$$C_{f_c} = \frac{C_f}{(1 + k\,M^2)^{.58}} \tag{4-12}$$

where $k = .15$ for no heat transfer and $k = .0512$ for cooled wall.

According to reference 10, the turbulent skin friction with roughness drops off according to the relation,

$$C_{f_c} = \frac{C_f}{1 + .18\,M^2} \tag{4-13}$$

However, this equation must be used with care. It is apparent the value of C_{f_c} calculated for the flow with roughness should never be less than the corresponding smooth value.

4.14 DRAG COEFFICIENT

Once the skin friction coefficient is determined, the skin friction drag coefficient, as based on reference area, is found by,

$$C_{D_f} = C_{f_c} \left(\frac{A_w}{A_r}\right) \tag{4-14}$$

For the fins, the wetted area of each fin is twice it's planform area. Thus, the tail skin friction drag coefficient is,

$$C_{D_{f_t}} = 2N\,C_{f_c} \left(\frac{A_T}{A_r}\right) \tag{4-15}$$

The body skin friction coefficient must be corrected for the fact that the body is not a flat plate, reference 6.

$$C_{D_{f_B}} = \left[1 + \frac{.5}{f_B}\right] C_{f_c} \frac{A_{w_B}}{A_r} \tag{4-16}$$

4.20 PRESSURE DRAG

4.21 TAIL PRESSURE DRAG

The pressure drag on a fin in subsonic flow arises from three basic contributions: a finite radius leading edge; thick trailing edge; and the overall fin thickness.
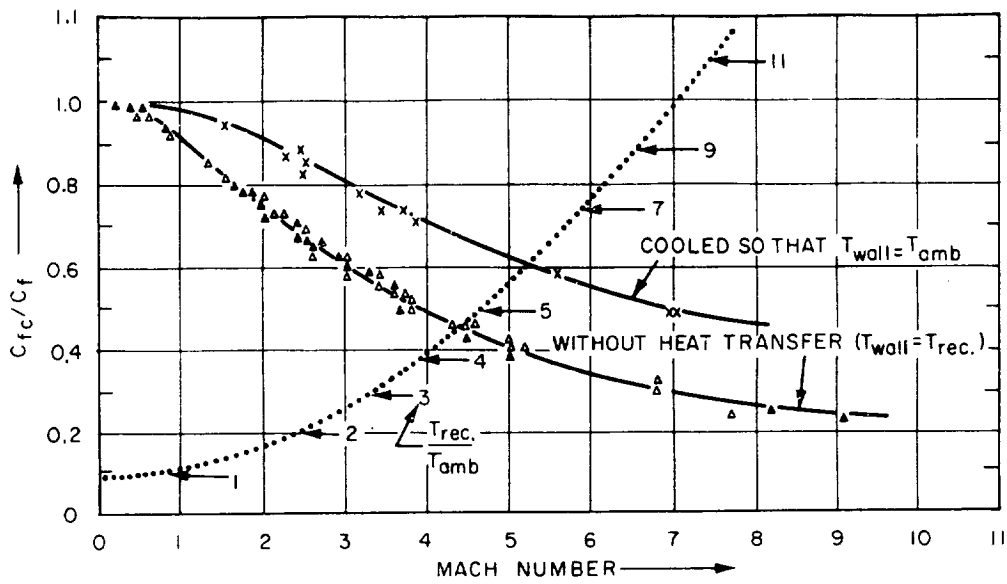
48

Figure 4-3—Supersonic C_{f_c} Variation

A finite radius leading edge can be considered a circular cylinder in cross flow that effectively has no base drag. Figure 4-4 from reference 6 shows the variation of the total drag coefficient of an infinite circular cylinder perpendicular to the flow and the variation of its base drag. The difference between these two curves is the drag coefficient of the leading edge. This difference is plotted in figure 4-5.

Subsonically up to M = .9 this curve is fitted by,

$$\Delta C_D = (1 - M^2)^{-.417} - 1 \quad (M < .9) \tag{4-17}$$

Between .9 $\leq$ M $\leq$ 1, the curve is essentially linear.

$$\Delta C_D = 1 - 1.5 \ (M - .9) \quad (.9 \leq M \leq 1) \tag{4-18}$$

Supersonically, the curve may be approximated by a high order polynomial, reference 6.

$$\Delta C_D = 1.214 - \frac{.502}{M^2} + \frac{.1095}{M^4} + \frac{.0231}{M^6} \quad (M > 1) \tag{4-19}$$

From cross flow theory, reference 6, the drag coefficient of a cylinder inclined to the flow is,

$$\frac{C_{D\angle}}{C_\perp} = \cos^3 \Gamma \tag{4-20}$$

The frontal area of a typical leading edge is;

$$A_{LE} = 2 \ L_{LE} \ r_L$$

the length can be expressed in terms of the span,

$$L_{LE} = \frac{S}{\cos \Gamma_L}$$

thus;

$$\frac{A_{LE}}{A_r} = \frac{2 \ S \ r_L}{A_r \cos \Gamma_L} \tag{4-21}$$

From equations 4-20 and 4-21, the total leading edge drag of N fins becomes,

$$C_{D_{L_T}} = 2N \left(\frac{S \ r_L}{A_r}\right) \cos^2 \Gamma_L \ (\Delta C_D) \tag{4-22}$$

where ΔC_D is obtained using equations 4-17 thru 4-19.

The trailing edge drag is two dimensional base drag and can be expressed in terms of the corrected skin friction coefficient, reference 5, for incompressible flow.

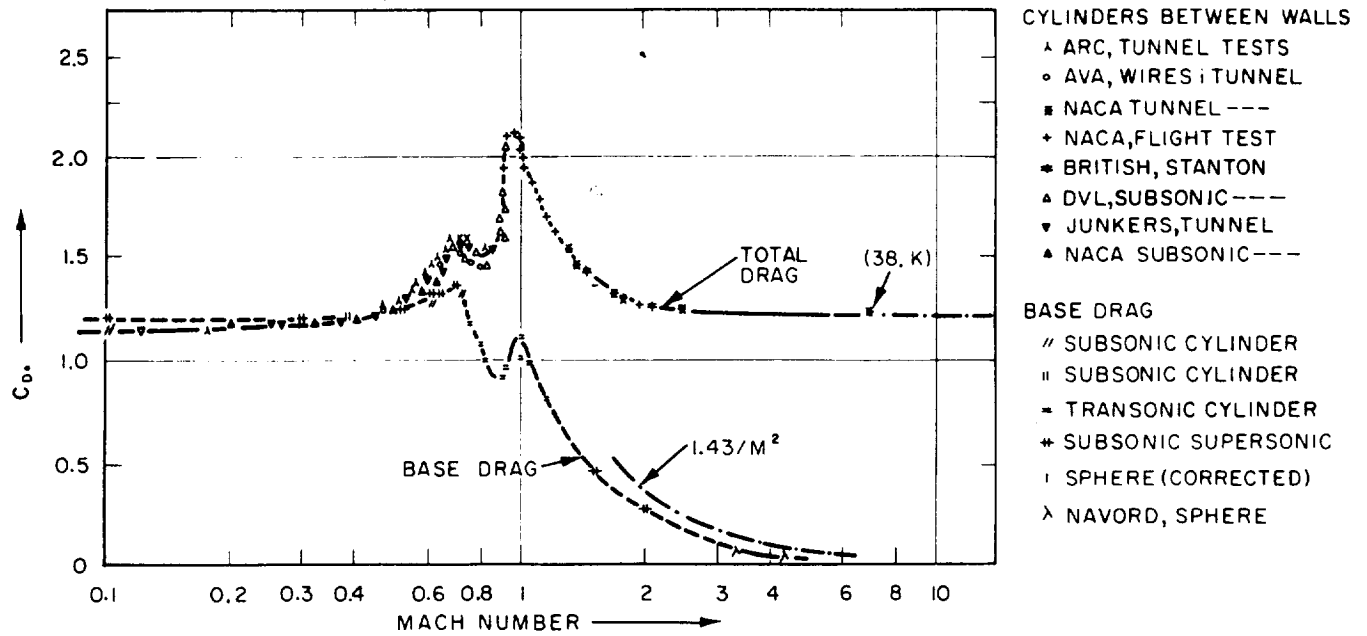$$C_{D_{B_T}} = \frac{0.135}{\sqrt[3]{C_{f_B}}} \tag{4-23}$$
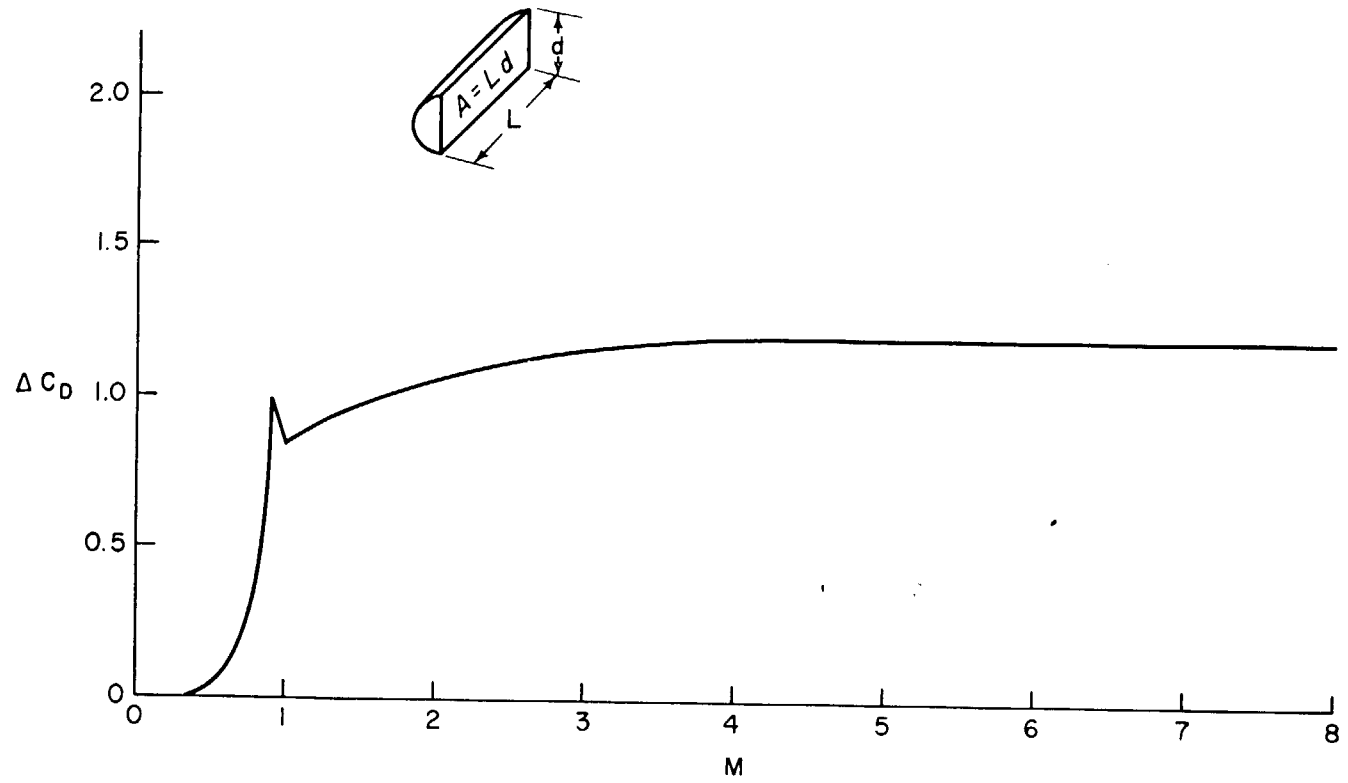
50

Figure 4-4—Cylinder Drag Variation

Figure 4-5—Leading Edge Drag

where;

$$C_{f_B} = 2 C_f \left(\frac{C_r}{h_r}\right)$$

(4-24)

For subsonic compressible flow, this may be corrected using the prandtl factor for swept wings, reference 6,

$$P_f = \frac{1}{\sqrt{1 - M^2 \cos^2 \Gamma_c}}$$

(4-25)

However, in order to maintain a finite value at

$$M^2 \cos^2 \Gamma_c = 1$$

the prandtl factor is corrected to,

$$P'_f = \frac{1}{\sqrt{K - M^2 \cos^2 \Gamma_c}}$$

(4-26)

where K is a constant to be determined from the value of $C_{D_{B_T}}$ at M = 1. Also, for compressible flow, equation 4-24 becomes,

$$C_{f_B} = 2 C_{f_c} \left(\frac{C_r}{h_r}\right)$$

(4-27)

After correcting to the reference area, the subsonic trailing edge drag coefficient for N fins is,

$$C_{D_{B_T}} = \frac{.135 N \left(\frac{A_{B_f}}{A_r}\right)}{\sqrt[3]{C_{f_B}} \sqrt{K - M^2 \cos^2 \Gamma_c}}$$

(4-28)

Reference 11 gives a curve for the two dimensional base pressure coefficient at supersonic speeds figure 4-6. This is essentially the base drag coefficient refered to the base area. An analytic expression which remains well within the cross hatching is,

$$P_B = \frac{1 - .52 \, M^{-1.19}}{M^2}$$

But, this must be corrected for possible boattailing of the fin, reference 6.

$$P_B = \frac{1 - .52 \, M^{-1.19}}{\left[1 + 18 C_{f_c} \left(\frac{t_r}{h_r}\right)^2\right] M^2}$$
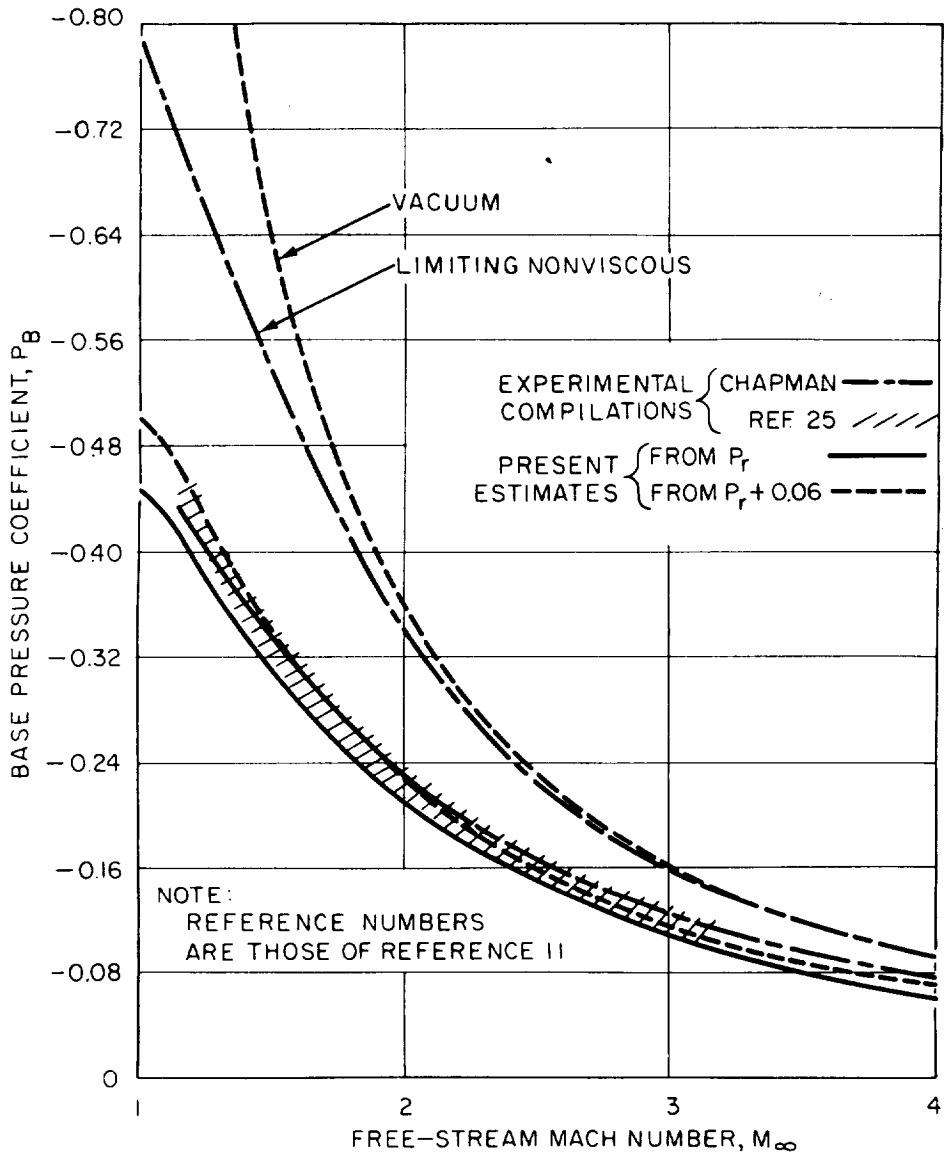
(4-29)

Figure 4-6—Two Dimensional Base Pressure

For N fins, the supersonic trailing edge drag coefficient, as corrected to the reference area is then,

$$C_{D_{B_T}} = \frac{N(1 - .52 \, M^{-1.19}) \left(\dfrac{A_{B_i}}{A_r}\right)}{\left[1 - 18 \, C_{f_c} \left(\dfrac{t_r}{h_r}\right)^2\right] M^2}$$

(4-30)

In order to determine the constant K, equations 4-28 and 4-30 are set equal at $M = 1$.

$$\frac{.135 \, N \left(\dfrac{A_{B_F}}{A_r}\right)}{\sqrt[3]{C_{f_c}} \sqrt{K - \cos^2 \Gamma_c}} = \frac{N(1 - .52) \left(\dfrac{A_{B_i}}{A_r}\right)}{\left[1 - 18 \, C_{f_c} \left(\dfrac{t_r}{h_r}\right)^2\right]}$$

where the superscript * indicates sonic values. Solving for K,

$$K - \cos^2 \Gamma_c = \frac{\left[.223 - 4.02 \, C_{f_c}^* \left(\dfrac{t_r}{h_r}\right)^2\right]^2}{\left[\left(\dfrac{t_r}{h_r}\right) C_{f_c}^*\right]^{2/3}}$$

(4-31)

This is used in equation 4-28 to evaluate the subsonic compressible trailing edge drag.

This method of maintaining finite values of the prandtl factor at mach one is used throughout the remaining derivations.

From reference 6, the drag due to thickness of two dimensional airfoil in compressible subsonic flow can be expressed as,

$$C_{D_{TT}} = C_{f_c} \left[4 \left(\frac{t}{c}\right) + \frac{120 \left(\dfrac{t}{c}\right)^4}{\left(\sqrt{1 - M^2}\right)^3}\right]$$

(4-32)

For a three dimensional fin, based on the reference area this becomes,

$$C_{D_{TT}} = C_{f_c} \left(\frac{A_T}{A_r}\right) \left[4 \left(\frac{t_r}{c_r}\right) + \frac{120 \left(\dfrac{t_r}{c_r}\right)^4}{\left(\sqrt{1 - M^2 \cos^2 \Gamma_c}\right)^3}\right]$$

(4-33)

55

Correcting it for a fin sweep and introducing the correction constant in the prandtl factor,

$$C_{D_{TT}} = C_{f_c} \left(\frac{A_T}{A_r}\right) \left[4\left(\frac{t_r}{c_r}\right) \cos \Gamma_c + \frac{120 \left(\frac{t_r}{c_i}\right)^4 \cos^2 \Gamma_c}{(K - M^2 \cos^2 \Gamma_c)^{3/2}}\right] \tag{4-34}$$

The value of the thickness drag of finite fins at mach one has been determined and presented in reference 6. A curve fit of the result is,

$$C_{D_{TT}}^* = 1.15 \left(\frac{t_r}{c_r}\right)^{5/3} \left[1.61 + \xi - \sqrt{(\xi - 1.43)^2 + .578}\right] \tag{4-35}$$

where

$$\xi = AR \left(\frac{t_r}{c_r}\right)^{1/3}$$

Solving 4-34 for K,

$$K = \cos^2 \Gamma_c + \left[\frac{\dfrac{C_{D_{TT}}^*}{C_{f_c}^*}\left(\dfrac{A_r}{A_T}\right) - 4\left(\dfrac{t_r}{c_r}\right) \cos \Gamma_c}{120 \left(\dfrac{t_c}{c_r}\right)^4 \cos^2 \Gamma_c}\right]^{2/3} \tag{4-36}$$

Equation 4-35 is used in 4-36 to determine K. The result is used in the following equation to determine the subsonic tail thickness drag. For N fins, equation 4-34 is;

$$C_{D_{TT}} = 4N C_{f_c} \left(\frac{A_T}{A_T}\right) \left[\left(\frac{t_r}{c_r}\right) \cos \Gamma_c + \frac{30 \left(\frac{t_r}{c_r}\right)^4 \cos^2 \Gamma_c}{\left(\sqrt{K - M^2 \cos^2 \Gamma_c}\right)^3}\right] \tag{4-37}$$

At supersonic speeds the effect of a finite radius leading edge is found by using equation 4-19 in equation 4-22. The trailing edge drag is calculated using equation 4-30. The thickness or wave drag, $C_{D_{W_T}}$, is computed by the method of reference 1 in appendix A.

The overall drag on the tail is the sum of the different contributions. In subsonic flow

$$\left(C_{D_T}\right)_T = C_{D_{f_T}} + C_{D_{L_T}} + C_{D_{B_T}} + C_{D_{TT}} \tag{4-38}$$

56

At supersonic speeds,

$$\left(C_{D_T}\right)_T = C_{D_{f_T}} + C_{D_{L_T}} + C_{D_{B_T}} + C_{D_{W_T}} \qquad (4\text{-}39)$$

Equation 4-38 uses the results from equations 4-15, 4-22, 4-28, and 4-37 respectively. Equation 4-39 uses equations 4-15, 4-22, 4-30, and results of appendix A respectively.

4.22 BODY PRESSURE DRAG

The body pressure drag may be broken down into two contributions, for body and base. According to reference 6, the forbody drag in subsonic compressible flow may be written,

$$C_{D_p} = \frac{6\, A_{W_B}\, C_{f_c}}{f_B^3\, A_r\, \left(\sqrt{1 - M^2}\right)^{1.2}} \qquad (4\text{-}40)$$

Again applying the correction constant to the prandtl factor,

$$C_{D_p} = \frac{6\, A_{W_B}\, C_{f_c}}{f_B^3\, A_r\, (K - M^2)^{.6}} \qquad (4\text{-}41)$$

From experimental data, reference 19, the forbody drag values of both ogives and cones are known, figure 4-7. In the range of values that are of interest, $1 \leq f_B \leq 10$, these curves may be fitted by the following equations.

$$\left(C_{D_p}^*\right)_{cone} = \frac{.88}{(f_N + .7)^{1.29}} \qquad (4\text{-}42)$$

$$\left(C_{D_p}^*\right)_{ogive} = \frac{.88}{(f_N + 1)^{2.22}} \qquad (4\text{-}43)$$

Solving equation 4-41 for K;

$$K = 1 + \left[\frac{6\, A_{W_B}\, C_{f_c}^*}{f_B^3\, A_r\, C_{D_p}^*}\right]^{5/3} \qquad (4\text{-}44)$$
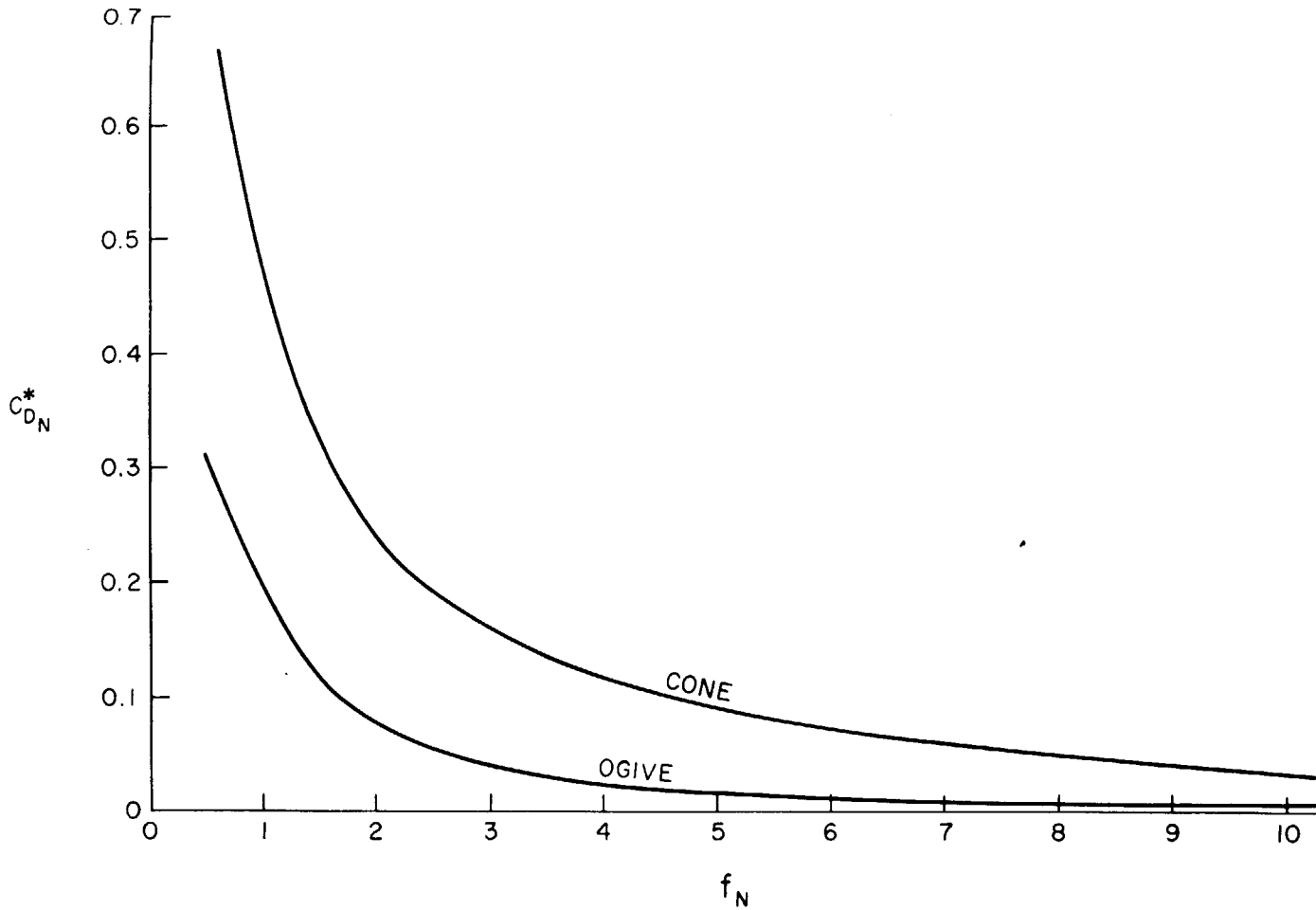
Figure 4-7—Nose Pressure Drag at Mach One

Then

$$K_{cone} = 1 + \left[\frac{6.82 \, A_{W_B} \, C_{f_c}^* \, (f_N + .7)^{1.29}}{f_B^3 \, A_r} \right]^{5/3} \qquad (4\text{-}45)$$

$$K_{ogive} = 1 + \left[\frac{6.82 \, A_{W_B} \, C_{f_c}^* \, (f_N + 1)^{2.22}}{f_B^3 \, A_r} \right]^{5/3} \qquad (4\text{-}46)$$

The subsonic compressible forbody pressure drag is found by using equations 4-45 or 4-46 in equation 4-41. For the nose $A_{W_{N_A}}$ and f_{N_A} should be used. For a conical shoulder $A_{W_{S_A}}$ and f_{S_A} are proper.

The supersonic value is determined by the second-order shock-expansion method, reference 27, as explained in section 3.21 of this thesis. The axial component of the pressure distribution is integrated around each element and then over the length of the body.

$$C_{D_P} = \frac{4}{\gamma M^2} \int_0^L \int_0^\pi P \sin \delta \, d\phi \, dx \qquad (4\text{-}47)$$

where

P comes from equation 3-69

δ = the local angle between the surface and the longitudinal axis

ϕ = Circumferential Angle.

The Base drag of a body of revolution in incompressible flow is presented in reference 5 as,

$$C_{D_B} = \frac{0.029}{\sqrt{C_{f_B}}} \qquad (4\text{-}48)$$

where,

$$C_{f_B} = C_f \left(\frac{A_W}{A_B} \right)$$

Correcting this to the reference area and for subsonic compressibility.

$$C_{D_B} = \frac{.029 \left(\frac{A_B}{A_r} \right)}{\sqrt{C_{f_c} \left(\frac{A_W}{A_B} \right) (1 - M^2)}} \qquad (4\text{-}49)$$

59

Introducing the correction constant into the prandtl factor term.

$$C_{D_B} = \frac{0.29 \left(\dfrac{A_B}{A_r}\right)}{\sqrt{C_{f_c} \left(\dfrac{A_w}{A_B}\right)} \ (K - M^2)}$$

(4-50)

From reference 11, for no fins near the body base, or for fins of zero thickness, the body base pressure coefficient at mach one is

$$P_B^* = 0.185$$

At mach one with $h_r/c_r = 0.1$,

$$P_B^* = 0.30$$

See figure 4-8.

The results of reference 11 indicate that P_B is roughly a linear function of fin trailing edge thickness at a constant mach number. Therefore,

$$C_{D_B}^* = \frac{A_B}{A_r} \left[0.185 + 1.15\left(\frac{h_r}{c_r}\right)\right]$$

(4-51)

Solving equation 4-50 for K,

$$K = 1 + \frac{\left[.029 \left(\dfrac{A_B}{A_r}\right)\right]^2}{C_{f_c}^* \left(\dfrac{A_w}{A_B}\right) (C_{D_B}^*)^2}$$

(4-52)

Using equation 4-51 in 4-52 and simplifying

$$K = 1 + \frac{1}{\left[6.38 + 39.7\left(\dfrac{h_r}{c_r}\right)\right] C_{f_c}^* \left(\dfrac{A_w}{A_B}\right)}$$

(4-53)

The subsonic compressible body base drag is computed by using equation 4-53 in 4-50.

References 11 and 6 both present curves of the base drag in supersonic flow. Figure 4-8 is from reference 11. The free flight test curve is most representative of the variation. It is an exponential over an initial range and an inverse square over the remainder of the mach numbers. To find the exponential, the free flight curve in figure 4-8 may be fitted in terms of the value at mach one.
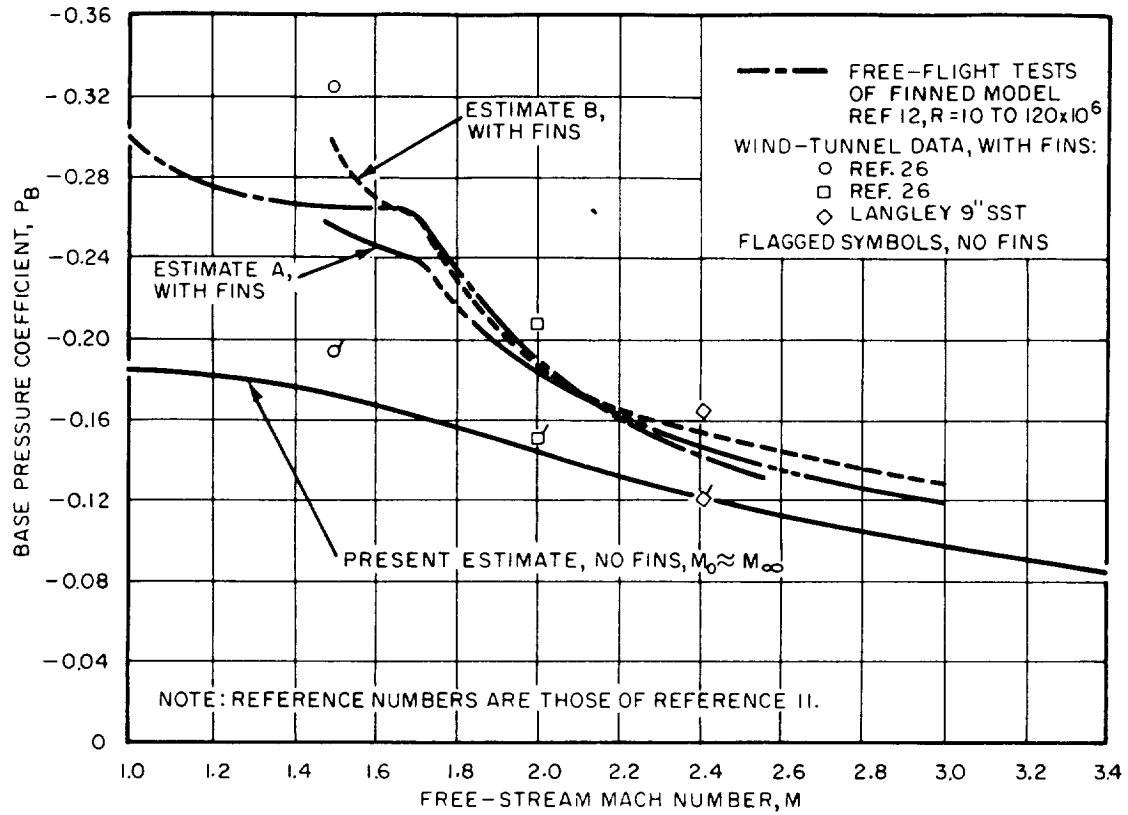
60

Figure 4-8—Three Dimensional Base Pressure

61

$$C_{D_B} = C_{D_B}^* \left[0.88 + .12\, e^{-3.58(M-1)} \right] \quad (1 \leq M \leq M_{cr}) \tag{4-54}$$

where M_{cr} is the point where the two variations cross. Also, reference 5 gives the inverse square variation as,

$$C_{D_B} = \frac{.7 \left(\dfrac{A_B}{A_r} \right)}{M^2} \quad (M > M_{cr}) \tag{4-55}$$

If it is assumed the ratio of the value of C_{D_B} at $M = M_{cr}$ to C^* remains constant for all curves, (inspection of the curves in reference 6 indicates this is a good assumption) then the value of the critical mach number can be found,

$$M_{cr} = \frac{0.892}{\sqrt{C_{D_B}^*}} \tag{4-56}$$

The value of $C_{D_B}^*$ is given by equation 4-51. In either subsonic or supersonic flow,

$$\left(C_{D_T} \right)_B = C_{D_P} + C_{D_{BB}} \tag{4-57}$$

For subsonic values, equation 4-41 and 4-50 are used. In supersonic flow equations 4-47 and 4-54 or 55 are used.

4.23 TOTAL DRAG

The drag of the total vehicle is the sum of the tail and body contributions.

$$C_D = \left(C_{D_T} \right)_T + \left(C_{D_T} \right)_B \tag{4-58}$$

No interference drag effects are considered.

5.00 COMPARISON WITH EXPERIMENTAL DATA

In an attempt to obtain as broad a range as possible without being voluminous, each characteristic is compaired to the data from a different configuration. In some cases, the choice of configuration was dictated by the availability of the appropriate data.

5.10 NORMAL FORCE COEFFICIENT DERIVATIVE AND CENTER OF PRESSURE

The windtunnel data of the Aerobee 350 sounding rocket, figure 5-1, are given in reference 14. Figures 5-2 and 5-3 show the results of the present method as well as data points from
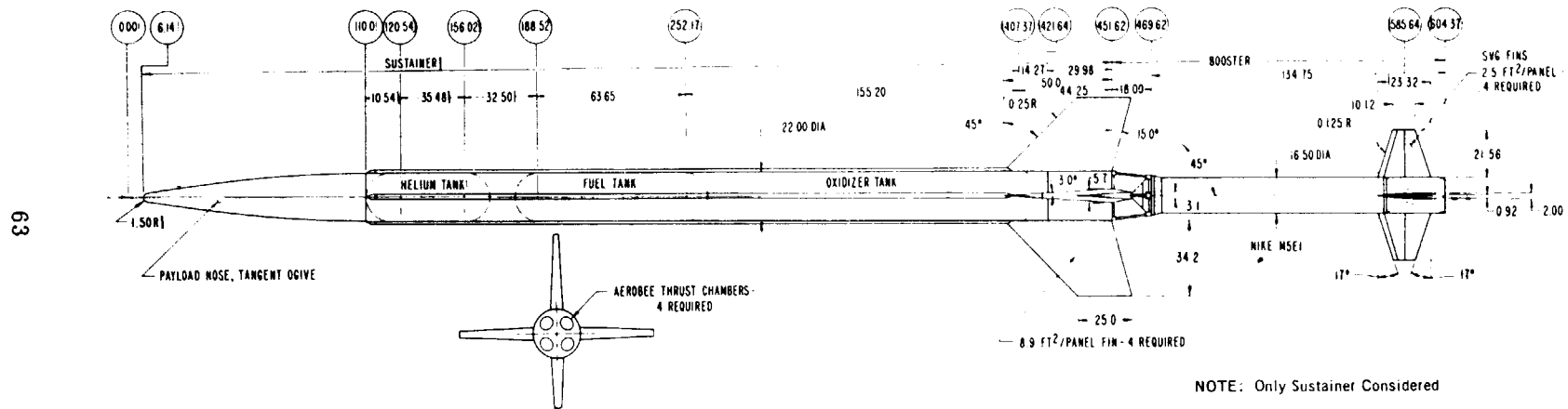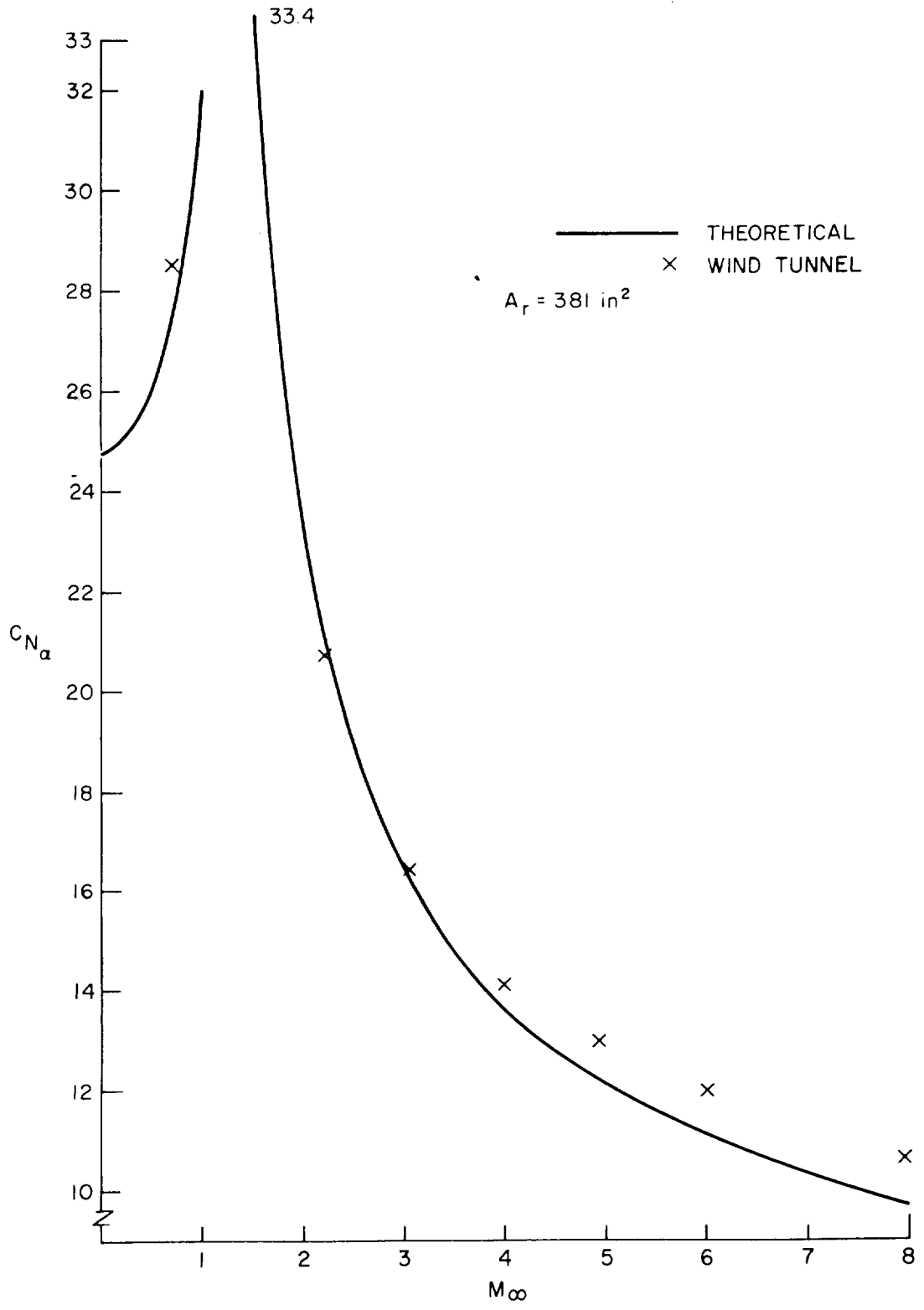
Figure 5-1—Aerobee 350

63

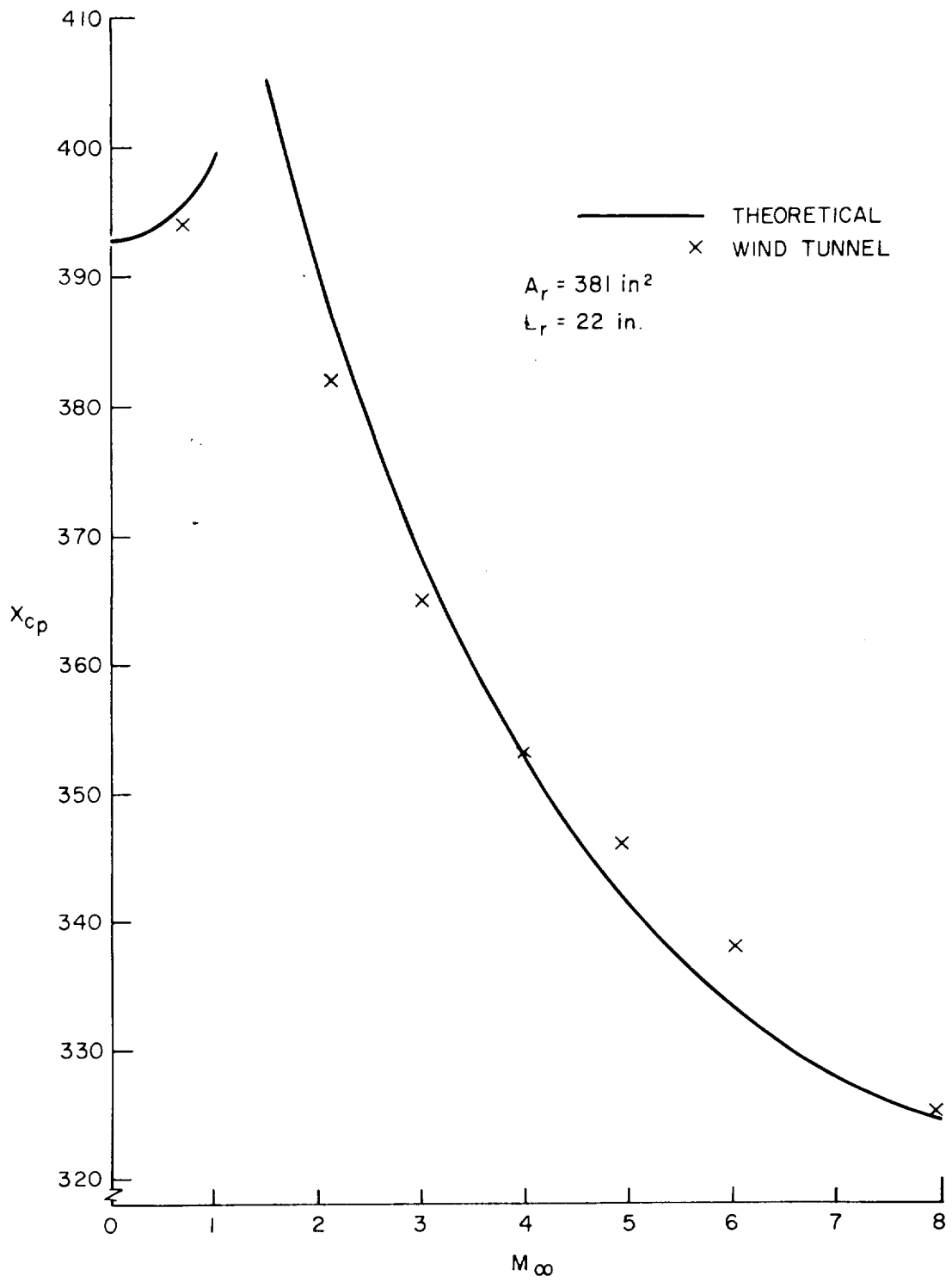Figure 5-2—Aerobee 350 Normal Force Derivative

Figure 5-3—Aerobee 350 Center of Pressure

65

reference 14. The maximum derivation of the theoretical C_{N_1} values is 7.83% and the maximum deviation of the theoretical center of pressure values is 1.18%. The degree of accuracy of the windtunnel tests is indicated as about 6%.

5.20 ROLL FORCING MOMENT COEFFICIENT DERIVATIVE

The only roll forcing moment coefficient derivative data over a broad range of mach numbers that are available to the author are those of the single stage tomahawk sounding rocket, figure 5-4. The data for this vehicle are unpublished at this time, but have been provided by the test coordinator, reference 28. Figure 5-5 shows the comparison between the theoretical result and windtunnel data. No data are available in the subsonic region. The average deviation of the theoretical C_{l_δ} is 7.54%. The accuracy of the windtunnel data is about 5%. It is apparent, both from the windtunnel data and the subsonic theory that the theoretical value at $M = 1.5$ is no good.

5.30 ROLL DAMPING DERIVATIVE

Reference 21 presents a full set of data for the basic finner test rocket, figure 5-6. It is the only configuration for which roll damping moment coefficient derivative data are available to the authors. Unfortunately, the range of the data is relatively small. Figure 5-7 shows the comparison between the theoretical C_{l_p} is 5.68%. Reference 21 does not indicate the degree of accuracy of its data. No subsonic data can be found for C_{l_p}.

5.40 DRAG COEFFICIENT

Aerobee 150A, figure 5-8, drag coefficient data are available from reference 29. The theoretical drag coefficient results are compared to the windtunnel data in figure 5-9. In order to duplicate the test conditions, the test reynolds numbers were used to set up a Re vs. M curve, figure 5-10. This curve was used in generating the theoretical data. The surface of the windtunnel model is highly finished. From table 4-1, the appropriate surface roughness is about .01 mils. The equivalent full scale surface roughness is .1 mils. The maximum deviation of the theoretical drag coefficient is 8.52%. Again no subsonic data are available.

5.50 PITCH DAMPING DERIVATIVE

There are no C_{m_q} experimental data available. The data taken in windtunnel experiments are a combination of the pitch damping derivative and a time log derivative due to the rate of change of angle-of-attack. There is no way to separate the two effects. Therefore, no comparison of the pitch damping derivative can be attempted.
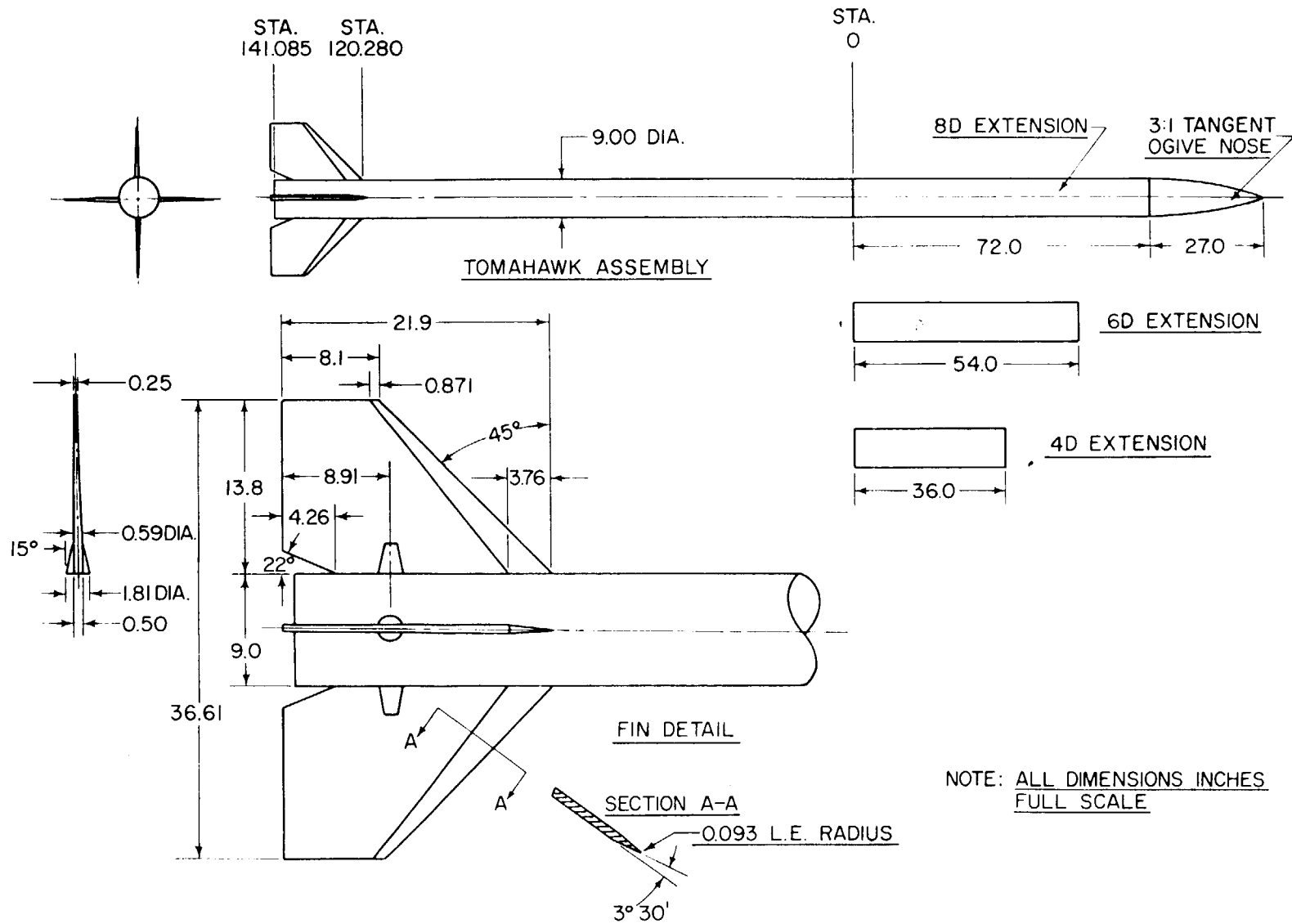
STA.   STA.
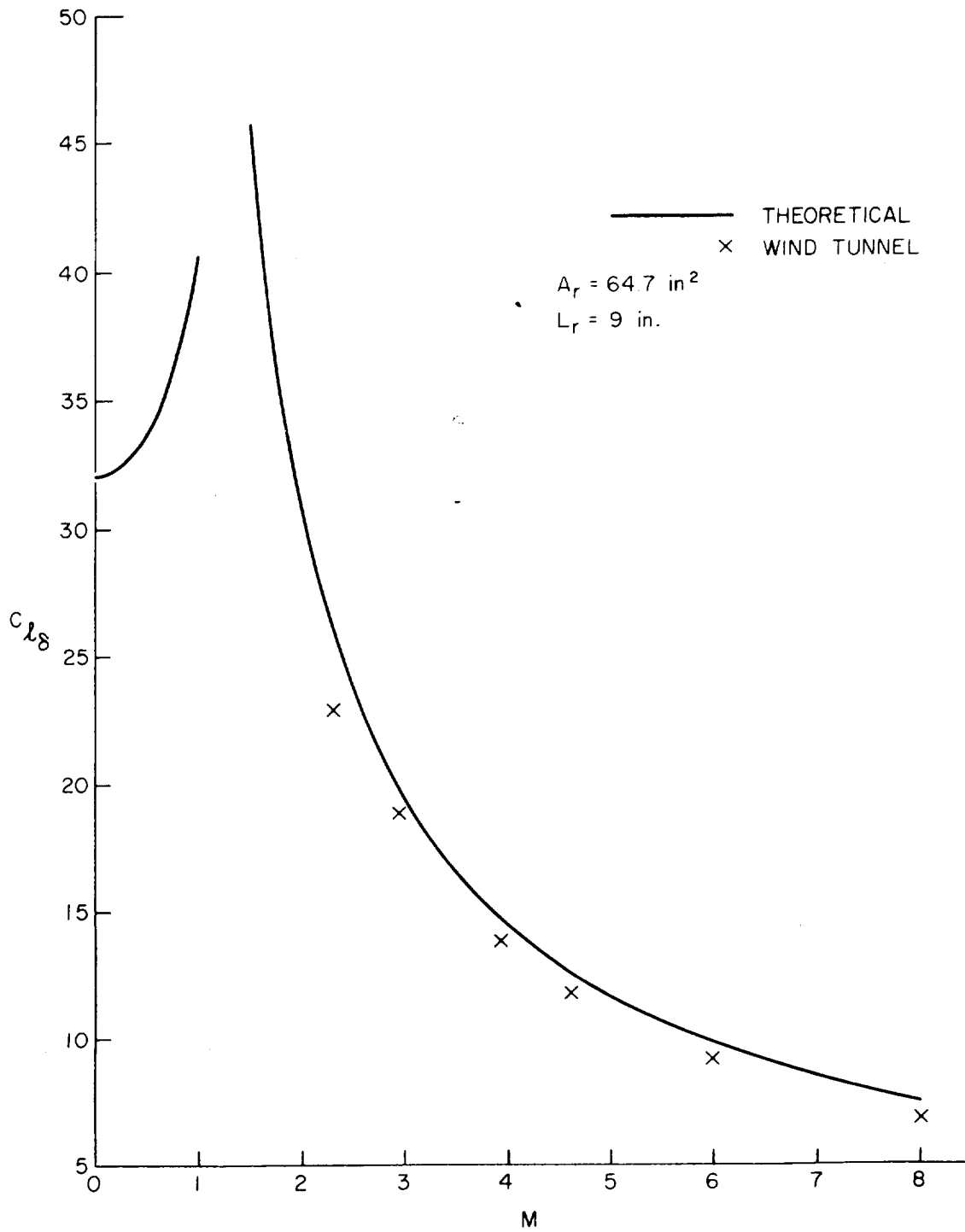141.085 120.280

STA.
0

9.00 DIA.

8D EXTENSION

3:1 TANGENT
OGIVE NOSE

TOMAHAWK ASSEMBLY

72.0

27.0

21.9

8.1

0.871

45°

3.76

8.91

13.8

4.26

22°

0.25

0.59 DIA.

15°

1.81 DIA.

0.50

9.0

36.61

6D EXTENSION

54.0

4D EXTENSION

36.0

A

A

FIN DETAIL

SECTION A-A

0.093 L.E. RADIUS

3° 30'

NOTE: ALL DIMENSIONS INCHES
FULL SCALE

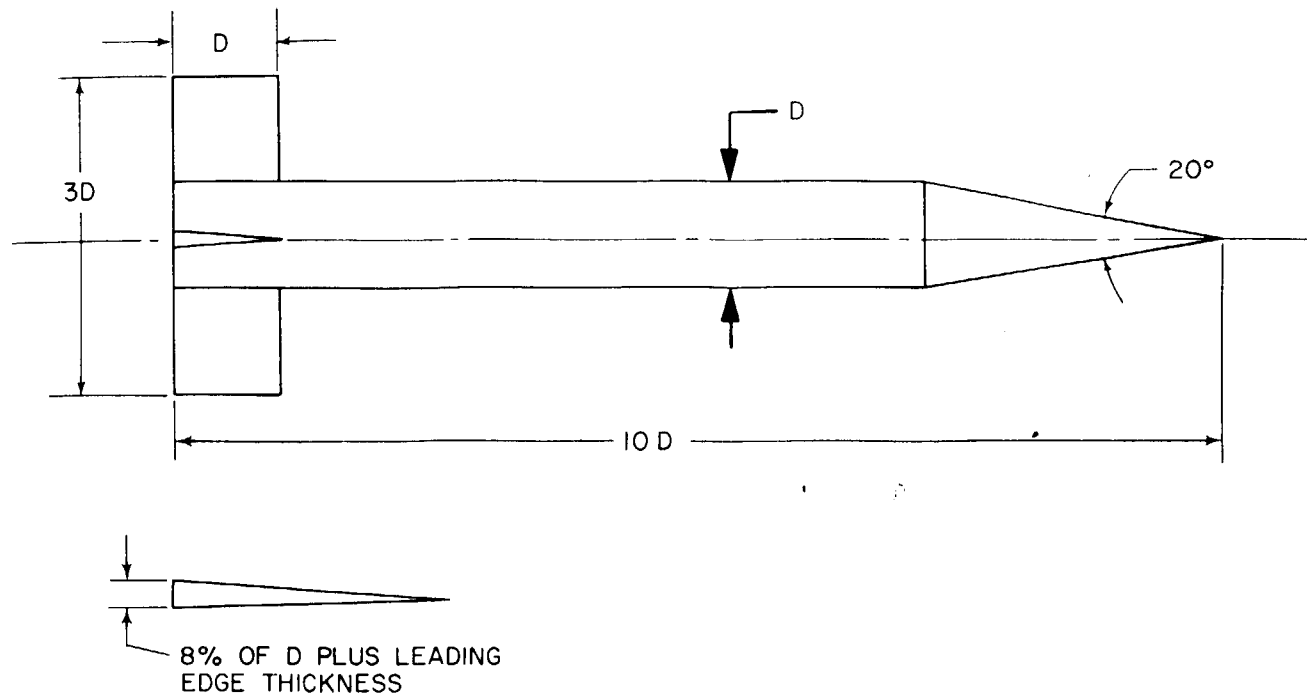Figure 5-4—Tomahawk

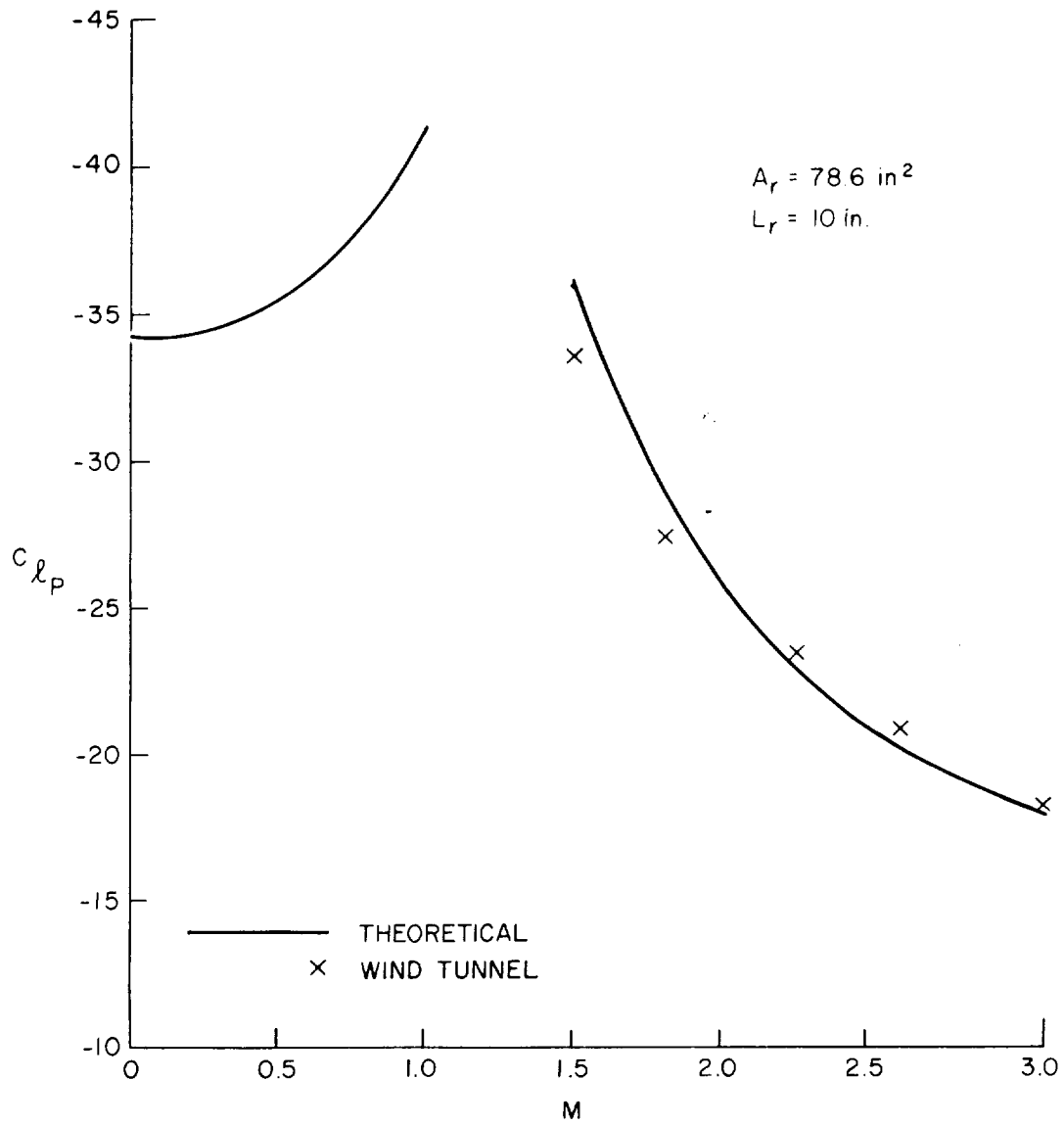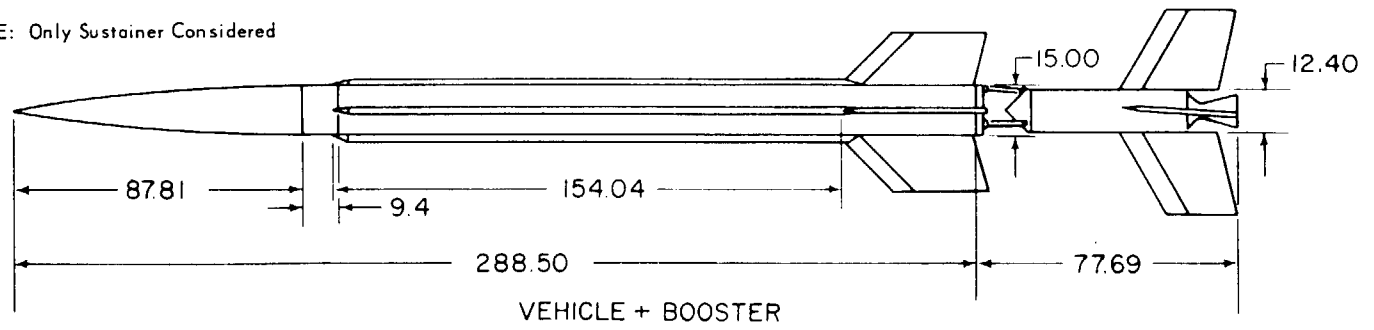Figure 5-5—Tomahawk Roll Forcing Derivative

Figure 5-6—Basic Finner

Figure 5-7—Basic Finner Roll Damping Derivative

NOTE: Only Sustainer Considered

15.00

12.40

87.81

9.4

154.04

288.50

77.69

VEHICLE + BOOSTER

28.00

45°

16.13

38.96

1.10

4°

SUSTAINER FINS

20.73

30°

23.50

27.68
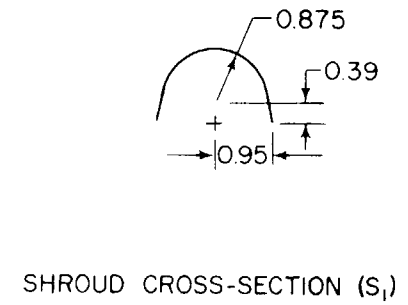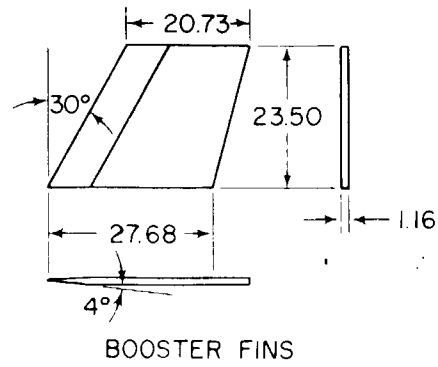
1.16

4°

BOOSTER FINS

0.875

0.39

0.95

SHROUD CROSS-SECTION (S_1)
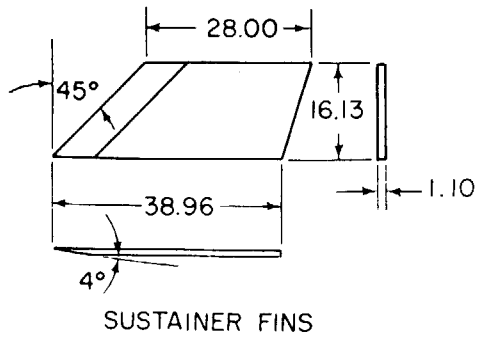
Figure 5-8—Aerobee 150A
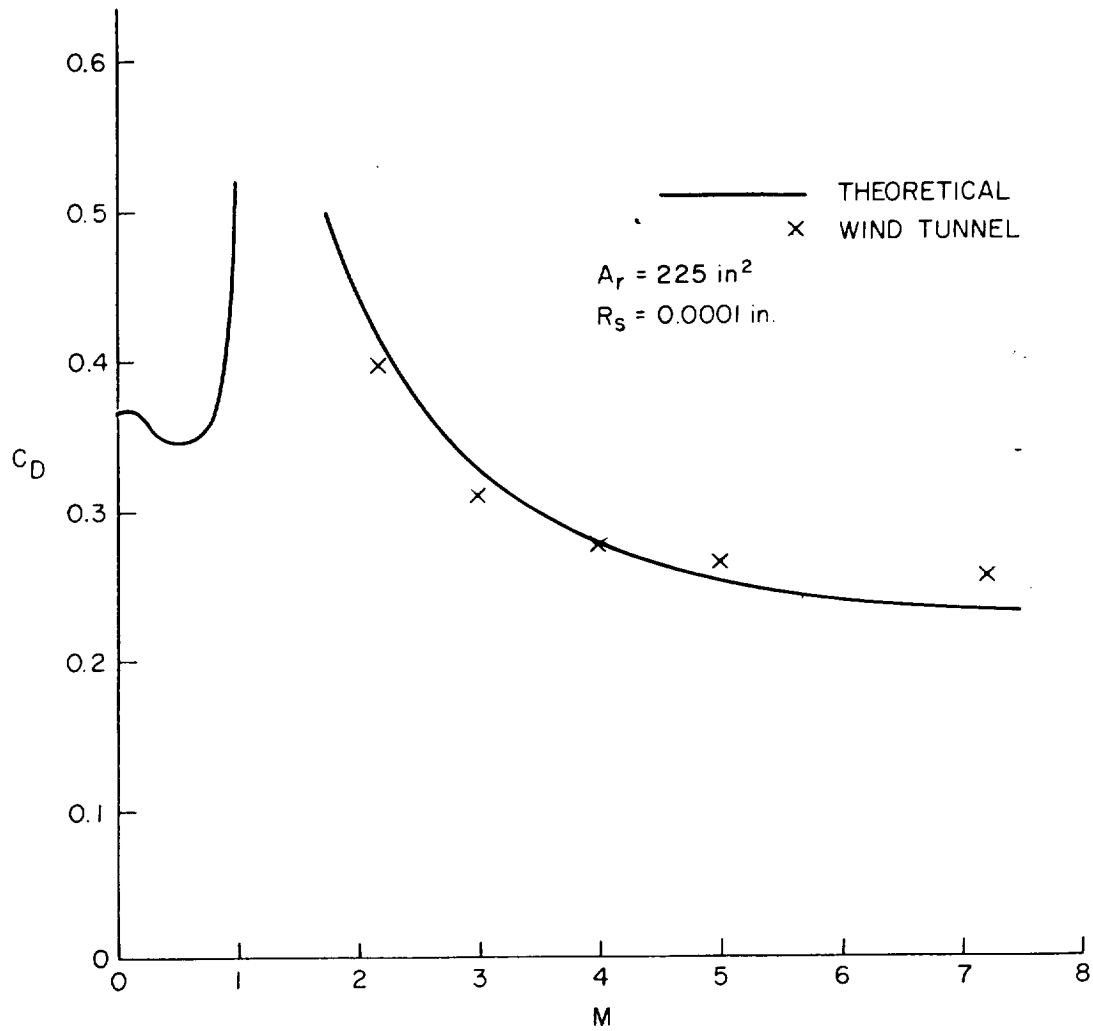
Figure 5-9—Aerobee 150A Drag Coefficient

72

X – VALUE USED IN
WIND TUNNEL TESTS
(REFERENCE 29)

THE SHAPE OF THE CURVE
IS FAIRED BY COMPARISON
WITH NOMINAL FLIGHT
REYNOLDS NUMBER
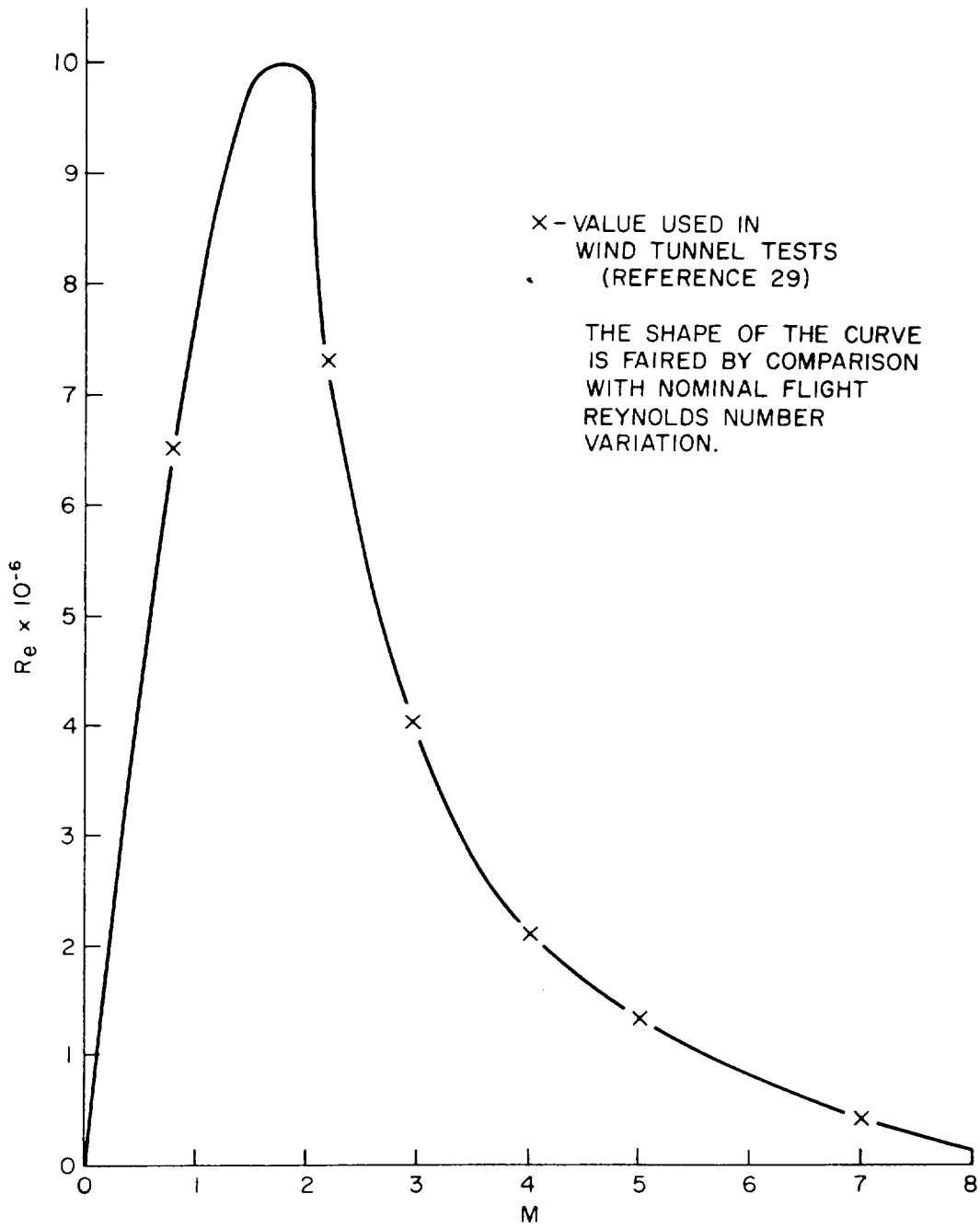VARIATION.

Figure 5-10—Aerobee 150A Reynolds Number

73

6.00 CONCLUSIONS

On the basis of the comparisons in section 5, the method presented in this dissertation presented in this dissertation predicts the values of C_{N_α}, $\bar{X}$, C_{ℓ_δ}, C_{ℓ_p}, and C_D to well within ten (10) percent of experimental results between mach 2 and 8. Although no comparison can be made for C_{mq}, the results of section 5-1, coupled with the dependence of C_{mq} on $(C_{N_\alpha})_{T(B)}$ and $\bar{X}_{T(B)}$, tend to indicate that the theoretical C_{mq} is also accurate to about 10%.

The lack of subsonic experimental data prevents any concrete conclusions to be drawn about the accuracy of the present method at subsonic speeds. However, the figures in section 5 show that the subsonic variations of all the compared characteristics are quite reasonably valued with respect to the supersonic values.

In general, then, the method presented in this dissertation can be used to confidently predict the aerodynamic characteristics of slender finned vehicles.

74

7.00 REFERENCES

1. Barrowman, J. S., FIN a Computer Program for Calculating the Aerodynamic Characteristics of Fins at Supersonic Speeds. NASA-GSFC X-721-66-162, 1966.

2. Diederich, F. W., A Plan Form Parameter for Correlating Certain Aerodynamic Characteristics of Swept Wings. NACA TN-2335, 1951.

3. Ferrari, C., Interference Between Wing and Body at Supersonic Speeds-Theory and Numerical Application. J. A. S., p. 317, June 1948.

4. Goldstein, S., Lectures on Fluid Mechanics. Interscience Publishers. New York, 1960.

5. Horner, S. F., Base Drag and Thick Trailing Edges. J. A. S., p. 622, October, 1950.

6. Horner, S. F., Fluid-Dynamic Drag. Published by the Author. Midland Park, N. J., 1958.

7. Jones, R. T., Properties of Low-Aspect-Ratio Pointed Wings at Speeds Below and Above the Speed of Sound. NACA Rep. 835, 1946.

8. Jones, R. T., Theory of Wing-Body Drag at Supersonic Speeds. NACA Report 1284, 1956.

9. Jones, R. T., and Cohen, D., High Speed Wing Theory, Princeton Univ. Press, Princeton, 1960.

10. Liepmann, H. W., Goddard, F. E., Note on the Mach Number Effects Upon the Skin Friction of Rough Surfaces. J. A. S., p. 784, October 1957.

11. Love, E. S., Base Pressure at Supersonic Speeds on Two-Dimensional Airfoils and on Bodies of Revolution With and Without Fins Having Turbulent Boundary Layers. NACA TN-3819, 1957.

12. Mayo, E. E., Cone Cylinder and Ogive Cylinder Geometric and Mass Characteristics. Memo to Code 721.2 Files, NASA-GSFC, 1965.

13. Mayo, E. E., Equations for Determining the Effects of Fin Dihedral on Vehicle Stability, Memo to Code 721.2 Files, NASA-GSFC, 1967.

14. McNerney, J. D., Aerobee 350 Windtunnel Test Analysis, Space General Corporation, ElMonte, California, 1963.

15. Miles, J. W., Unsteady Supersonic Flow. Section 12.4 A.R.D.C., Baltimore, 1955.

16. Moore, L. L., Yound, G. B. W., Jansen E., Compressible Boundary Layer-Laminar Solution, J. A. S., p. 229, April, 1952.

17. Morikawa, G., Supersonic Wing-Body Lift. J. A. S., Vol. 18, No. 4, April, 1951, pp. 217-228.

18. Morikawa, G. K., The Wing-Body Problem for Linearized Supersonic Flow. PhD Thesis, California Inst. of Tech., 1949.

19. Morris, D. N., A Summary of the Supersonic Pressure Drag of Bodies of Revolution. J. A. S., p. 622, July 1961.

20. Murk, M. M., The Aerodynamic Forces on Airship Hulls. NASA Report 184, 1924.

21. Nicolaides, J. D., Missile Flight and Astrodynamics, BuWeps TN-100A, Washington, D. C., 1959.

22. Nielsen, J. N., and Pitts, W. C., Wing-Body Interference at Supersonic Speeds with an Application to Combinations with Rectangular Wings. NACA TN-2677, 1952.

23. Pitts, W. C., Nielsen, J. N., and Kaattari, G. E., Lift and Center of Pressure of Wing-Body-Tail Combinations at Subsonic, Transonic, and Supersonic Speeds. NACA Report 1307, 1959.

24. Sims, J. L., Tables for Supersonic Flow Around Right Circular Cones at Small Angles-of-Attack. NASA SP-3007, 1964.

25. Sims, J. L., Tables for Supersonic Flow Around Right Circular Cones at Zero Angle-of-Attack, NASA SP-3004, 1964.

26. Shapiro, A. H., The Dynamics and Thermodynamics of Compressible Fluid Flow, Vol. II, Ronald Press, New York, 1954.

27. Syverston, C. A., and Dennis, D. H., A Second-Order Shock-Expansion Method Applicable to Bodies of Revolution Near Zero Lift, NACA Report 1328, 1957.

28. Thomas, C. G., Unpublished Windtunnel Data on a .25 Scale Tomahawk Sounding Rocket Taken at LRC Unitary and ARDC Tunnel B, October 1966.

29. Thomas, E. S., Windtunnel Tests of the Aerobee 150A. Aerojet-General Corporation, Azusa, California, April 1960.

30. Tsien, H. S., Supersonic Flow Over an Inclined Body of Revolution, JAS, p. 480, Vol. 5, 1938.

APPENDIX A

FIN

A COMPUTER PROGRAM FOR CALCULATING THE AERODYNAMIC
CHARACTERISTICS OF FINS AT SUPERSONIC SPEEDS
(Exerpt of Theoretical Treatment)

James S. Barrowman
Spacecraft Integration and Sounding Rocket Division

April 1966

Goddard Space Flight Center
Greenbelt, Maryland

LIST OF SYMBOLS

A Reference area

c Length of airfoil strip chord

C_{DW} Wave drag coefficient $= \dfrac{F_d}{qA}$

C_L Lift coefficient $= \dfrac{F_l}{qA}$

$C_{L\alpha}$ $dC_L/d\alpha \ (\alpha = 0)$

C_l Rolling moment coefficient $= \dfrac{Mr}{qAL}$

C_{l_δ} $dC_l/d\delta \ (\delta = 0)$

C_m Pitching moment coefficient $= \dfrac{Mp}{qAL}$

C_{m_α} $dC_m/d\alpha \ (\alpha = 0)$

C_{P_i} Local pressure coefficient

C_r Length of root chord

d_i Component of l_i parallel to the freestream

d_w Portion of d_i behind the fin-tip Mach cone

F_d Drag force (parallel to freestream)

F_l Lift force (normal to freestream)

K Interference factor

L Reference length

l_L Length of airfoil-strip leading-edge region chord

l_{L_r} Length of root airfoil leading-edge region chord

l_M Length of center region and of center-region chord

l_T Length of airfoil-strip trailing-edge region chord

l_{T_r} Length of root airfoil trailing-edge region chord

l_w Distance between the leading edge and the intersection of the Mach cone with the airfoil strip

l_i Length of local region surface

M Freestream Mach number

M_p Pitching moment about the reference axis

LIST OF SYMBOLS (Continued)

M_r	Rolling moment about the root chord
n	Number of strips
n_i	Component of 1_i normal to the freestream
P_i	Local static pressure
P_n	Ambient static pressure
q_v	Freestream dynamic pressure
r_i	d_w/d_i ratio
S	Semispan length
X_L	Distance from the reference axis to the airfoil-strip leading edge in a streamwise direction
$\bar{X}$	Center-of-pressure coordinate measured from the reference axis
x_{P_i}	Distance from the reference axis to the forward region boundary of a local region in a streamwise direction
$\bar{Y}$	Center-of-pressure coordinate measured from the root chord
y	Distance from the root chord in a spanwise direction
$\triangle y$	Width of airfoil strip
α	Angle of attack (degree)
β	$\sqrt{M^2 - 1}$
Γ_L	Leading-edge sweep angle
Γ_T	Trailing-edge sweep angle
Γ_1, Γ_2	Region boundaries sweep angles
γ	Ratio of specific heats for air = 1.4
δ	Fin cant angle
ζ_L	Leading-edge wedge half-angle in the streamwise direction
ζ_T	Trailing-edge wedge half-angle in the streamwise direction
η	Inclination of a local surface to the freestream
μ	Mach cone semivertex angle

SUBSCRIPTS

B	Body alone
B(T)	Body in the presence of the tail
i	Local region number
j	Airfoil strip number

79

SUBSCRIPTS

o   Value at $\alpha = 0$

T   Tail alone

T(B)   Tail in the presence of the body

FIN

A COMPUTER PROGRAM FOR CALCULATING THE AERODYNAMIC CHARACTERISTICS OF FINS AT SUPERSONIC SPEEDS

BACKGROUND

Calculating the aerodynamic characteristics of the fins of a sounding rocket is one of the basic steps in calculating the overall aerodynamics of a sounding rocket. Because sounding rockets fly at supersonic speeds for the greater portion of their flight, the regime at these speeds is of particular interest.

Methods previously used for calculating supersonic fin aerodynamics (references 1, 2, 3, and 4) are lacking in accuracy and applicability because of the many assumptions and approximations inherent in using them to reach a closed form or nearly closed form solution.

By using a high-speed computer to numerically solve basic theoretical equations, one may obtain answers rapidly and as accurately as desired. The only restrictions to accuracy are the assumptions inherent in deriving the basic equations. The theory found to be most amenable to programming in Busemann's Second Order Supersonic Airfoil Theory as described in reference 1.

PROGRAM CAPABILITIES AND LIMITATIONS

Given a supersonic fin with chord plane symmetry, at a given Mach number, FIN computes as functions of angle of attack ( ) the following:

- Lift coefficient, C_L
- Wave drag coefficient, C_{DW}
- Pitching moment coefficient, C_m
- Center-of-pressure coordinate measured from the reference axis, $\bar{X}$
- Center-of-pressure coordinate measured from the root chord, $\bar{Y}$

Since as defined in the program is equivalent to the fin cant angle (δ) at $\iota = 0$, the rolling moment coefficient C_l is considered a function of δ.

FIN also computes as functions of Mach number the following:

- Lift coefficient slope, C_{L_ι}
- Wave drag at zero angle of attack, C_{DW_o}
- Pitching moment coefficient slope, C_{m_ι}
- Rolling moment coefficient slope, C_{l_δ}

81

- Center-of-pressure coordinate measured from the reference axis at zero angle of attack, $\bar{X}_0$

- Center-of-pressure coordinate measured from the root chord at zero angle of attack, $\bar{Y}_0$

The range of α is from zero to α_{max}, as determined by the user, in increments of 1 degree. The program allows for a maximum of 100 Mach number points, the user specifying the range and increment of the Mach number.

Since FIN has been designed for use with a four-finned vehicle, the output values of C_L, C_{DW}, C_m, C_{L_α}, C_{DW_0}, and C_{m_α} are for a pair of identical fins; the output values of C_l and C_{l_δ} are for two pairs of perpendicular fins. The values of $\bar{X}$, $\bar{Y}$, $\bar{X}_0$, and $\bar{Y}_0$ apply only to a single typical fin.

Busemann's Second Order Airfoil Theory is applied subject to the restrictions outlined in reference 1, pages 192 to 241, with special attention to Figures 10.3 and 10.28. However, the use of the third-order terms in this program slightly enlarges the applicability shown in this reference. Busemann's theory is applied to small streamwise airfoil strips, and the strips are summed in a spanwise direction. In addition, the fin-tip Mach cone is accounted for by applying a correction factor to the necessary portion of each strip. This correction-factor technique was obtained from references 1 and 3. The fin-tip Mach cone correction may or may not be included at the user's discretion.

Figure 1 shows the types of fins to which FIN is applicable. These configurations cover all of the shapes normally used on sounding rockets and missiles. The program input pattern for each type is given in the section on usage. A listing of FIN in FORTRAN IV is given in Appendix A.

AERODYNAMIC THEORY

Busemann's Second Order Airfoil Theory has been applied to two-dimensional airfoil strips with the following assumptions:

- All parts of the airfoil surface are in supersonic flow and make small angles with the flow. This implies low angles of attack.

- The leading edge is sharp. The trailing edge must be sharp for a double wedge fin or a modified double wedge. For a single wedge and a modified single wedge, the effect of the blunt base is neglected.

- The shock waves are all attached.

- Each region of flow over the surface acts independently of the others.

The basic local pressure coefficient equation of the Busemann theory is a third-order series expansion:

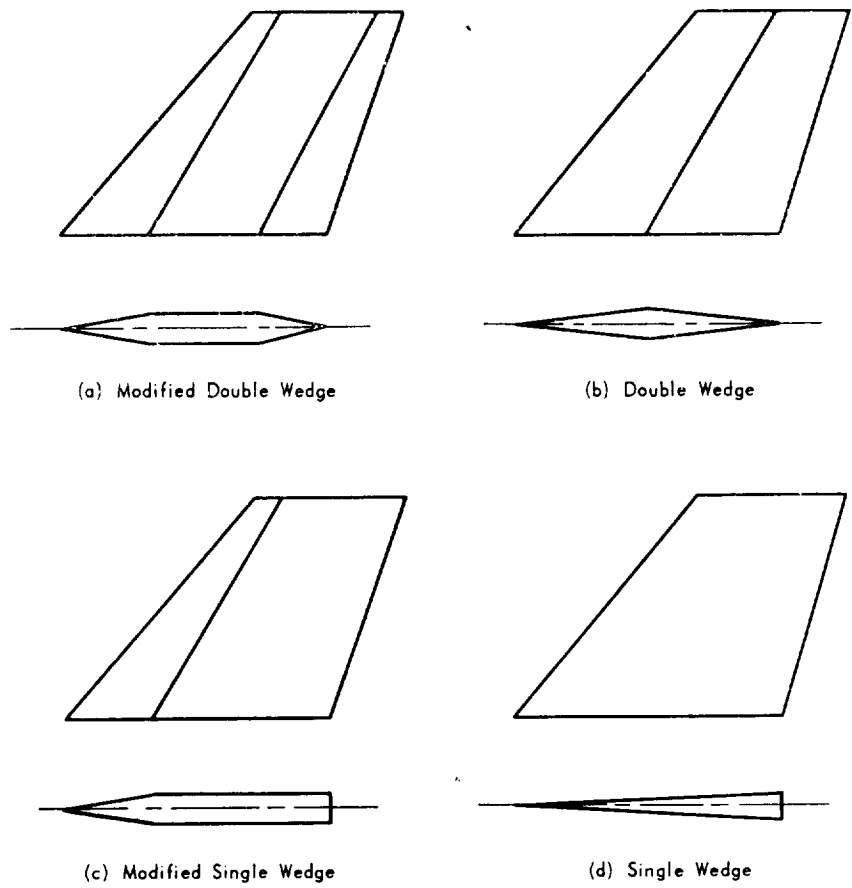$$C_{P_i} = \frac{P_i - P_\infty}{q_\infty} = K_1 \eta_i + K_2 \eta_i^2 + K_3 \eta_i^3 - K^* \eta_L^3 \tag{1}$$

(a) Modified Double Wedge

(b) Double Wedge

(c) Modified Single Wedge

(d) Single Wedge

Figure 1—Fin Configurations

where

$$K_1 \cdot \frac{2}{?} \tag{2a}$$

$$K_2 = \frac{(\gamma + 1)M^4 - 4\gamma^2}{4\gamma^4} \tag{2b}$$

$$K_3 \cdot \frac{(\gamma + 1)M^8 + \left(2\gamma^2 - 7\gamma - 5\right)M^6 + 10(\gamma - 1)M^4 - 12M^2 + 8}{6\gamma^7} \tag{2c}$$

If the flow over the surface region inclined at η_i to the flow has been preceded by a single compressive shock wave anywhere upstream in the flow, the value of κ^* is:

$$\kappa^* \cdot \frac{(\gamma + 1)M^4 \left[(5 - 3\gamma)M^4 + 4(\gamma - 3)M^2 + 8\right]}{48} \tag{3}$$

If the flow upstream of the region in question has contained only expansive shock-free flow, $\kappa^* = 0$. η_L is the inclination of the leading edge surface. Essentially, the first three terms of equation 1 represent the first-, second-, and third-order pressures on the surface region respectively. The κ^* term is the third-order irreversible pressure rise through the bow shock. The index, i, indicates the surface for which the pressure coefficient is being calculated.

The pressure coefficient of equation 1 is applied to a typical airfoil region, including the fin-tip Mach cone, by dividing the region into two portions at the intersection of the airfoil strip and the Mach cone (Figure 2). A correction factor of $1/2$ is applied to the local pressure coefficient for the region within the Mach cone. The center of pressure of each portion is taken as the midpoint of the length of that portion. By this means, equations are obtained for the local lift (F_{l_i}), drag (F_{d_i}), local center of pressure ($\bar{x}_i$), and, hence, the local pitching moment (M_{p_i}):

$$F_{l_i} = C_{P_i} \, d_i \left(1 - \frac{r_i}{2}\right) \tag{4}$$

$$F_{d_i} = C_{P_i} \, n_i \left(1 - \frac{r_i}{2}\right) \tag{5}$$

$$\bar{x}_i = \frac{\tfrac{1}{2}d_i \left[1 - r_i + \frac{r_i}{2} + \frac{x_{P_i}}{1_i}(2 - r_i)\right]}{1 - \frac{r_i}{2}} \tag{6}$$

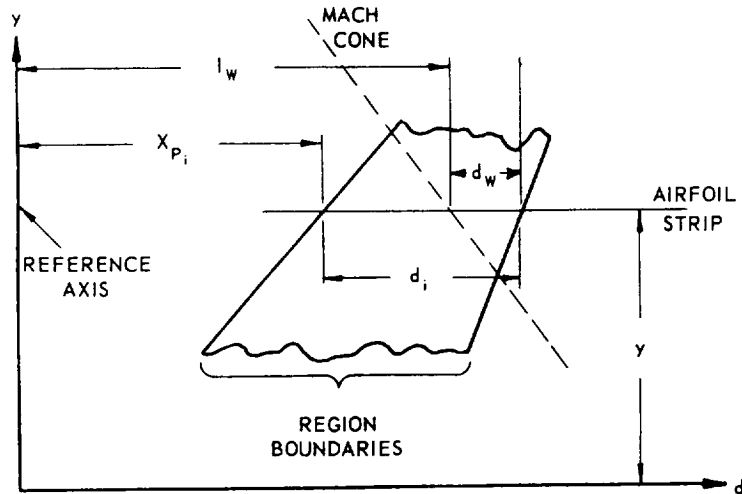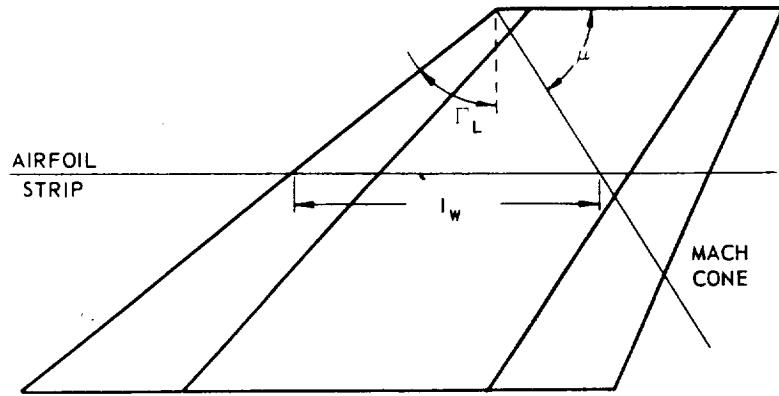$$M_{p_i} = F_{l_i} \, \bar{x}_i \tag{7}$$

84

Figure 2—Mach Cone Correction Geometry

The airfoil-strip lift (F_{l_j}), drag (F_{d_j}), and pitching moment (M_{p_j}) totals are then computed by summing the local characteristics.

$$F_{l_j} = \sum_{i=1}^{6} F_{l_i} \qquad (8)$$

$$F_{d_j} = \sum_{i=1}^{6} F_{d_i} \qquad (9)$$

$$M_{p_j} = \sum_{i=1}^{6} M_{p_i} \qquad (10)$$

The strip rolling moment about the root chord is calculated from the airfoil lift and strip spanwise position, y:

$$M_{r_j} = y F_{l_j} \qquad (11)$$

The total characteristics over the entire fin are then computed by summing the airfoil strip characteristics in a spanwise direction.

$$F_l = \sum_{j=1}^{n} F_{l_j} \qquad (12)$$

$$F_d = \sum_{j=1}^{n} F_{d_j} \qquad (13)$$

$$M_p = \sum_{j=1}^{n} M_{p_j} \qquad (14)$$

$$M_r = \sum_{j=1}^{n} M_{r_j} \qquad (15)$$

The forces and moments computed in equations 4 through 15 are actually divided by the ambient dynamic pressure (q_∞) and strip width (Δy). Thus, the associated coefficients are:

$$C_L = \frac{2F_1 \cdot \Delta y}{A} \quad \text{(2 fins)} \tag{16}$$

$$C_{DW} = \frac{2F_d \cdot \Delta y}{A} \quad \text{(2 fins)} \tag{17}$$

$$C_m = \frac{2M_p \cdot \Delta y}{AL} \quad \text{(2 fins)} \tag{18}$$

$$C_l = \frac{4M_r \cdot \Delta y}{AL} \quad \text{(4 fins)} \tag{19}$$

The center-of-pressure coordinates are calculated from the respective moments and the appropriate lift forces.

$$\bar{X} = \frac{M_p}{F_1 \cos \alpha} \tag{20}$$

$$\bar{Y} = \frac{M_r}{F_1} \tag{21}$$

To obtain the linear slope coefficients near $\alpha = 0$ at a given Mach number, the values of C_L, C_m, and C_l are calculated at $\alpha = 1°$ and are taken as the slope values C_{L_α}, C_{m_α}, and C_{l_δ} (all per degree). The slope values per radian are obtained by the proper conversion of radians to degrees. Thus:

$$\frac{C_{L_\alpha}}{\text{rad.}} = \frac{180}{\pi}\left(C_L\big|_{\alpha = 1}\right) \tag{22}$$

$$\frac{C_{m_\alpha}}{\text{rad.}} = \frac{180}{\pi}\left(C_m\big|_{\alpha = 1}\right) \tag{23}$$

$$\frac{C_{l_\delta}}{\text{rad.}} = \frac{180}{\pi}\left(C_l\big|_{\delta = 1}\right) \tag{24}$$

The zero angle-of-attack values of C_{DW}, $\bar{X}$, and $\bar{Y}$ are simply their respective values at $\alpha = 0$.

CONFIGURATION AND GEOMETRY CONSIDERATIONS

The user indicates the shape of the fin configuration by specifying the root chord length (c_r), root airfoil leading and trailing edge region chord lengths (1_{Lr} and 1_{Tr}), leading and trailing edge

sweep angles (Γ_L and Γ_T), region boundary sweep angles (Γ_1 and Γ_2), and the fin semispan length (S) (Figure 3). The program then computes the distance from the reference axis to the airfoil-strip leading edge in the streamwise direction (X_L), airfoil chord length (C), and the airfoil region chord lengths (1_L and 1_T) as functions of the spanwise coordinate of the airfoil strip.

$$X_L = y \tan \Gamma_L \cos \iota \tag{25}$$

$$C = y \left(\tan \Gamma_T - \tan \Gamma_L \right) + C_r \tag{26}$$

$$1_L = y \left(\tan \Gamma_1 - \tan \Gamma_L \right) + 1_{L_r} \tag{27}$$

$$1_T = y \left(\tan \Gamma_T - \tan \Gamma_2 \right) + 1_{T_r} \tag{28}$$

The width of the airfoil strip is determined from the number of strips (n) desired by the user.

$$\Delta y = \frac{S}{n} \tag{29}$$

The airfoil strip crossection is assumed to be symmetrical about the chord line. The most general crossection configuration is the modified double wedge (Figure 1a). The other three types (Figures 1b, 1c, and 1d) are special cases of this basic shape. Figure 4 shows in detail the general crossection, which has six separate flow regions. As can be seen in this figure, the surface region lengths are determined by specifying the leading- and trailing-edge wedge half angles in the stream-wise direction, ζ_L and ζ_T.

$$1_1 = 1_4 = \frac{1_L}{\cos \zeta_L} \tag{30}$$

$$1_3 = 1_6 = \frac{1_T}{\cos \zeta_T} \tag{31}$$

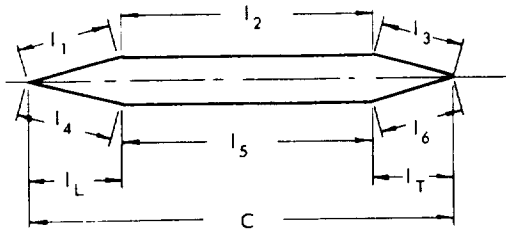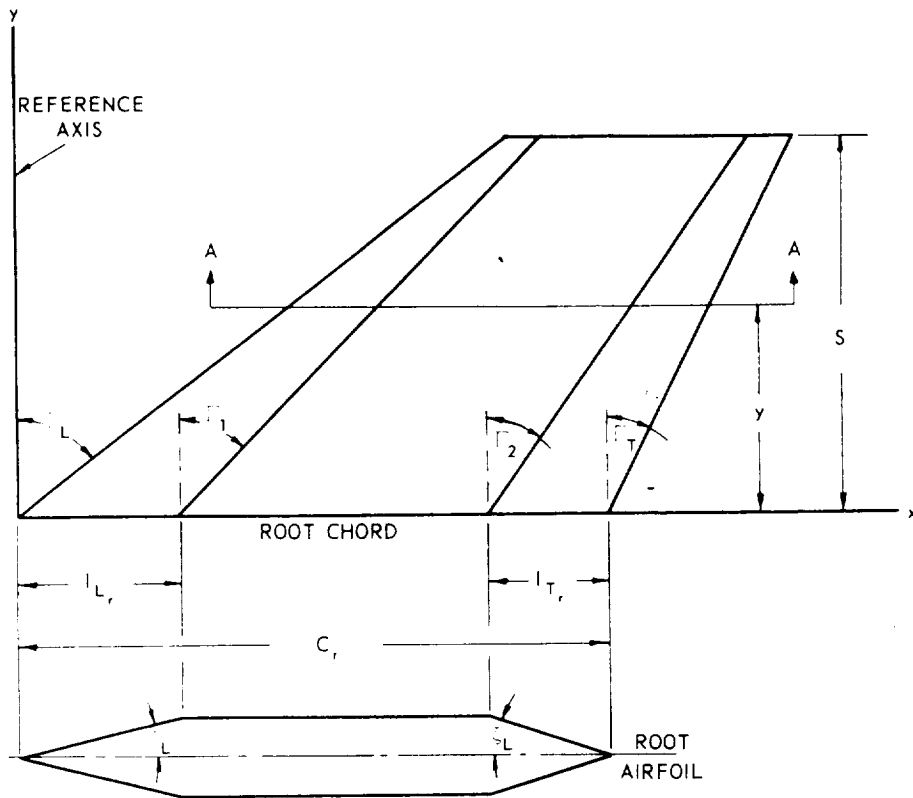$$1_2 = 1_5 = C - 1_L - 1_T \tag{32}$$

The program computes the local-surface inclination angles (η_i) as functions of α:

$$\eta_1 = \zeta_L - \alpha \tag{33a}$$

$$\eta_2 = - \alpha \tag{33b}$$

$$\eta_3 = - \zeta_T - \alpha \tag{33c}$$

$$\eta_4 = \zeta_L + \alpha \tag{33d}$$

88

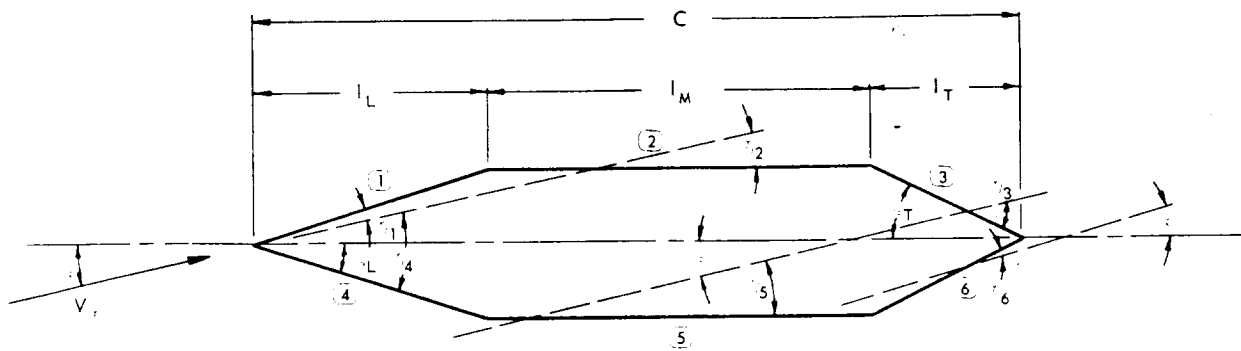SECTION A-A   TYPICAL AIRFOIL

Figure 3—Fin and Airfoil Geometry

89

Figure 4—Airfoil Angles

$$\eta_5 = \iota \tag{38e}$$

$$\eta_6 = \zeta_T + \alpha \tag{38f}$$

From these, the streamwise and normal components of the region lengths are calculated.

$$d_i = l_i \cos \eta_i \quad (i = 1 \to 6)$$

$$n_i = l_i \sin \eta_i \quad (i = 1 \to 6) \tag{34}$$

The distance of the forward local-region boundaries from the reference axis are then determined as:

$$x_{P1} = x_{P4} = X_L \tag{35a}$$

$$x_{P2} = X_L + d_1 \tag{35b}$$

$$x_{P3} = X_L + d_1 + d_2 \tag{35c}$$

$$x_{P5} = X_L + d_4 \tag{35d}$$

$$x_{P6} = X_L + d_4 + d_5 \tag{35e}$$

FIN-TIP MACH CONE CORRECTION

The Mach-cone angle (μ) is a direct function of the Mach number.

$$\mu = \text{Arctan} \left(\frac{1}{\beta}\right) = \text{Arcsin} \left(\frac{1}{M}\right) \tag{36}$$

For an airfoil strip at a spanwise direction y, the intersection of the strip and the Mach cone is a distance l_w from the leading edge.

$$l_w = (S - y) \tan \zeta_L + \tan(90 - \mu) \tag{37}$$

But, by trigonometric identities and the use of equation 37, this may be reduced to:

$$l_w = (S - y) \left(\tan \zeta_L + \beta\right) \tag{38}$$

If l_w is greater than or equal to the chord length, there is, of course, no actual intersection and no correction is necessary. If l_w is such that

$$C > l_w \geq C - l_T$$

91

then the ratio of the portion of l_T falling behind the Mach cone to l_T is:

$$r_3 = r_6 = \frac{C - l_w}{l_T} \qquad (39)$$

Also,

$$r_1 = r_2 = r_4 = r_5 \quad 0 \qquad (40)$$

If l_w is such that

$$C - l_T > l_w \geq l_L$$

then the corresponding ratio for the middle regions is

$$r_2 = r_5 \quad \frac{C - l_T - l_w}{l_M} \qquad (41)$$

Also,

$$r_3 \quad r_6 \quad 1 \qquad (42a)$$

and,

$$r_1 \quad r_4 \quad 0 \qquad (42b)$$

If l_w is such that

$$C - l_T - l_M \quad l_w \geq 0$$

then the ratio for the leading edge region is

$$r_1 \quad r_4 = \frac{l_L - l_w}{l_L} \qquad (43)$$

Also,

$$r_2 \quad r_3 \quad r_5 \quad r_6 \quad 1.0 \qquad (44)$$

These ratios are the values used in equations 4, 5, and 6 for calculating the local lift, drag, and center of pressure. In these equations, the pressure coefficient in the portion behind the Mach cone is taken as half the value of the C_p calculated by equation 1.

REFERENCES

1. Hilton, W. F., High Speed Aerodynamics. Longmans, Green and Co. New York, 1951.

2. Pitts, W. C., Nielsen, J. N. and Kaattari, G. E., Lift and Center of Pressure of Wind-Body-Tail Combinations at Subsonic, Transonic, and Supersonic Speeds. NACA Report 1307, 1959.

3. Shapiro, A. H., The Dynamics and Thermodynamics of Compressible Fluid Flow. Vol. II. Ronald Press. New York, 1954.

4. Harmon, S. M. and Jeffreys, I., Theoretical Lift and Damping in Roll of Thin Wings with Arbitrary Sweep and Taper at Supersonic Speeds Supersonic Leading and Trailing Edges. NACA TN 2114. May 1950.

5. Thomas, E. S., Windtunnel Tests of the Aerobee 150A. Aerojet General Corp., 1960.

6. McNerney, J. D., Aerobee 350 Windtunnel Test Analysis. Space General Corp. January 1963.